EFFECTS OF ELEMENT ELEVATION AND POSITION ERRORS ON THE RESPONSE OF SEISMIC ARRAYS

BY

RYAN ADHI PUTRA

A Thesis Presented to the

DEANSHIP OF GRADUATE STUDIES

KING FAHD UNIVERSITY OF PETROLEUM & MINERALS

DHAHRAN, SAUDI ARABIA

In Partial Fulfillment of the
Requirements for the Degree of

MASTER OF SCIENCE

In

GEOPHYSICS

DECEMBER 2017

KING FAHD UNIVERSITY OF PETROLEUM & MINERALS

DHAHRAN- 31261, SAUDI ARABIA

DEANSHIP OF GRADUATE STUDIES

This thesis, written by **RYAN ADHI PUTRA** under the direction of his thesis advisor and approved by his thesis committee, has been presented and accepted by the Dean of Graduate Studies, in partial fulfillment of the requirements for the degree of **MASTER OF SCIENCE IN GEOPHYSICS.**

Dr. Abdullatif Al-Shuhail

(Advisor)

Dr. Abdulaziz Al-Shaibani

(Department Chairman)

Dr. Abdulaziz Al-Shaibani

(Member)

Dr. Salam A. Zummo

Dean of Graduate Studies

Dr. SanLinn Ismail Kaka

(Member)

4/3/18

Date

© RYAN ADHI PUTRA

2017

This study is dedicated to my mother. She fought the battle with her illness while I lived on another side of the world and fortunately I could be there when she passed away. Thank you for your love, support, encouragement, and all of the beautiful things you had done for me and made me who I am Today.

ACKNOWLEDGMENT

In the name of Allah, the Almighty, for the blessing and mercy that had given me the opportunity and capability to complete my studies at King Fahd University of Petroleum and Minerals (KFUPM). Peace and Blessing of Allah be upon our Prophet Muhammad, his families, and his companions.

I acknowledge, with deep gratitude and appreciation, to my thesis advisor, Dr. Abdullatif Al- Shuhail for his encouragement, knowledge, guidance, patience, and support that he has given to me over the past few years since the beginning of my study at KFUPM.

I would like to thank for the support and knowledge to Dr. Abdulaziz Al-Shaibani, as chairman of Geosciences Department and thesis committee member, and Dr. SanLinn Ismail Kaka, as graduate coordinator and thesis committee member. My appreciation also goes to other faculty members and staff of Geosciences Department for their support, knowledge, and hospitality.

Finally, I am very grateful to my family; my wife, my parents, and my sisters for their support, patience, and encouragement during my academic journey.

TABLE OF CONTENT

LIST OF TABLES

LIST OF FIGURES

ABSTRACT

Full Name : Ryan Adhi Putra

Thesis Title : Effects of element elevation and position errors on the response of seismic arrays

Major Field : Geosciences

Date of Degree : December 2017

Seismic arrays are systematic arrangements of seismic receivers, sources or both. Seismic receiver array response is the sum of the outputs of the receivers in an array. The purpose of using seismic receiver arrays is to enhance the signal-to-noise ratio (S/N) by attenuating the undesired horizontally traveling surface waves such as ground roll. The combined effects with variations of element's weights, positions, and elevations on the seismic receiver arrays response were addressed in this study. These variations are common especially in areas with rugged topography. The objective of this research is to quantify the degradation in the wavelet response of a seismic array caused by the combination of these errors on a 12-element equally weighted geophone array with various elements' spacing and wavelet incidence angle.

The effects of errors were modeled using zero-mean Gaussian random errors in element's weights, positions, and elevations with 10% and 20% standard deviations. The average from 32 times calculation for each standard deviations was used to obtain statistically significant results.

The ideal array response and perturbed array response were compared through the calculation of their trace energies. As expected, the combination of errors degraded the

array response more as compared to individual errors. However, it did not denote that the degradation of combined errors was the total of each single error. Taking the 45^{o} incidence angle as an example, the minimum array response in the ideal case has a trace energy of -43 dB which occurs at a temporal element spacing of 0.054 s. The addition of 10% combined errors degrades the minimum array response by about 17%; while 20% combined errors degrade it by 30%. Therefore, the results of this research indicate that the effects of combined errors are significant and care must be taken in planting arrays as close to the ideal case as possible when acquiring seismic data.

Furthermore, the methodology was applied on a seismic real data set acquired over a sandstone in eastern Saudi Arabia. The degradation in trace energy of the real data was only 1.29% as opposed to 38.24% degradation predicted by the proposed method. This discrepancy might be attributed to noise, statics, and wavelet issues present in the real data.

ملخص الرسالة

الاسم الكامل : ريان اضحي بوترا

عنوان الرسالة : آثار ارتفاع الجيوفونات و أخطاء التموقع على استجابة المصفوفات الزلزالية.

التخصص :علم أرض

تاريخ الدرجة العلمية : ديسمبر ٢٠١٧

المصفوفات الزلزالية هي عبارة عن ترتيبات نظامية من مصادر أو مستقبلات زلزالية او كلاهما. مصفوفة المستقبلات الزلزالية (مصفوفة الجيوفونات) هي مجموع مخرجات المستقبلات (الجيوفونات) في المصفوفة. الهدف من استخدام مصفوفات المستقبلات الزلزالية هو تحسين نسبة الاشارة الى الضجيج بتقليص الموجات السطحية المتحركة أفقيا الغير مرغوب بها مثل التدحرج الأرضي. أثر تغيرات أوزان ومواقع وارتفاعات الجيوفونات على استجابات مصفوفات المستقبلات الزلزالية سيتم مناقشته في هذه الدراسة. هذه المتغيرات شائعة خاصة في المناطق ذات التضاريس الوعرة والعوائق كالشجر. الهدف من هذا البحث هو تحديد كمية الانحطاط في استجابة المويجة من المصفوفة الزلزالية بسبب هذه المجموعة من الأخطاء على مصفوفة جيوفونات ذات 12 جيوفون متساوية الأوزان مع عناصر متنوعة البعد وزاوية سقوط المويجة.

آثار الأخطاء تمت نمذجتها باستعمال أخطاء ذات توزيع عشوائي غاوسي و متوسط صفري في أوزان ومواقع وارتفاعات الجيوفونات مع 10% و 20% انحرافات معيارية. للحصول على نتائج ذات معنى احصائيا تم اخذ المعدل من 32 مرة لكل انحراف معياري.

استجابة المصفوفة المثالية و ذات الأخطاء تمت مقارنتهما بحساب طاقات مساراتهما. كما هو متوقع، مجموعة الأخطاء ستحط من استجابة المصفوفة أكثر من الأخطاء الفردية. ولكن هذا لايعني أن الانحطاط من مجموعة أخطاء هو مجموع انحطاط كل خطأ على حدة. فلنأخذ زاوية سقوط 45 درجة مثالا، أقل استجابة مصفوفة في الحالة المثالية لديه 43- dB ويحدث عند تباعد جيوفون زمني يقدر ب 0.054 ثانية. اضافة 10% أخطاء مجتمعة تحط استجابة المصفوفة الأقل 17%، بينما 20% أخطاء مجموعة تحط من الاستجابة 30%. لذلك تستنتج من نتيجة هذا البحث أن

آثار الأخطاء المجموعة جديرة بالاعتبار ويجب الحرص على وضع المصفوفات باقرب حالة من المثالية قدر المستطاع.

بالإضافة إلى ذلك فقد تم تطبيق الطريقة على بيانات سايزمية حقيقية كان قد تم جمعها من على حجر رملي في المنطقة الشرقية من المملكة العربية السعودية. كان تفاوت الطاقات باستخدام البيانات الحقيقية (1.29%) خلافا ل (38.24%) المتوقعة باستخدام الطريقة المقترحة. قد يكون هذا الفرق حدث بسبب الضجيج و مسائل أخرى موجودة في البيانات الحقيقية.

CHAPTER 1

INTRODUCTION

Seismic arrays are a group of seismic receivers (geophones), sources, or even both planted in a systematic arrangement. This research only concentrated on seismic receiver (geophone) arrays. Seismic arrays are used to suppress noise in the field. Many of the existing studies on seismic arrays assumed ideal array by considering it has perfect element weights, perfect implementation conditions, and homogeneous earth. However, these assumptions are rarely satisfied in the field, hence limiting the applicability of the results of these studies. Furthermore, within certain field conditions, several aspects such as mentioned above influence the response of receiver arrays. The outcome responses attained from the non-ideal field were different as compared to the ideal state. All of the aspects may decrease the effectiveness of multi-channel processing and its waveform [1].

Rost and Thomas (2002) presented several applications of seismic arrays. Originally, seismic arrays were developed to monitor nuclear explosions [2]. The studies of nuclear explosion identification are closely related to studies of the seismic source, especially to distinguish between a natural earthquake and nuclear explosion [3] [4]. Kárason and van der Hilst (2001) explained that seismic arrays improved the Earth's interior velocity models through the use of large number and dense spatial samples of the seismic wavefield at several locations on the Earth's surface [5]. In terms of reflection seismology, the main purpose of an array of geophones is to increase the signal-to-noise ratio (S/N) by enhancing the desired signals (reflections) and attenuating seismic noise during the acquisition of seismic data in the field. As the desired seismic signals travel across the array with a much higher horizontal velocity, thus these signals produce a longer

wavelength, as compared to that of unwanted signals [6]. The desired signals are usually those that have been reflected from deep geologic horizons, hence they are considered as normal incident angle wave. The unwanted signals are considered as random and incoherent or coherent surface waves generated by the source such as ground roll. Thus, a geophone array can also be considered as a directional filter [7]. Understanding the variation in field parameters affecting the seismic array response is an important step in the acquisition, processing, and interpretation of the seismic data.

1.1. Literature review

Seismic arrays response is commonly represented in many terms, such as time-harmonic, incident, and plane waves. Many authors analyzed seismic arrays utilizing the time-harmonic-wave, namely Newman and Mahoney (1973), Smith (1956), Savit et al. (1958), and others. They investigated the effects of noise, geophone positioning, and weighting errors on the array responses. Their findings were very useful, however, they did not explain the response from seismic arrays for the impulsive signal. A few of known impulsive signals include Klauder or Ricker wavelets, which are commonly used in seismic exploration.

Smith (1956) showed a general concept of arrays. He used time-harmonic analysis to explain the array response disrupted by the variations in velocity, dip, and elevation within the array length. He found that high frequency from the incident wave is affected by the changes in elevation within the array length [8].

White (1958) described a method for the computation of the expected waveform from close-spaced pattern of shots or geophones when the individual signal is a pulse [9].

He studied the effects of array weighting functions on the performance of seismic array. Furthermore, he analyzed the case of incident plane waves and compared the effects of several source array weighting functions, such as equal, triangular, and one-half cycle sinusoid functions.

Newman and Mahoney (1973) presented their study regarding the result of errors in position and weighting. They used plane time-harmonic waves as the incident wave with different weight variable. They concluded that the wavelet response was proportionally degraded to the complexities of the weighting function [10].

Johnson and Dudgeon (1993) revealed the relation between signal processing and arrays [11]. They showed that errors in gain or position have an effect on the array response. They further concluded that position errors exerted more damage than gain errors.

Gangi and Benson (1989) explained the wavelet response due to errors in weights and position of the elements of the geophone arrays with respect to several variables. These variables include the type and nominal error added, number of the elements used, and weighting function [12]. Gangi and Benson (1989) revealed that the degradation of the wavelet response is a function of a number of elements in the array and weighting function. A similar case was investigated by Al-Shuhail and Gangi (1994), wherein they evaluated the alteration in the array response caused by elevation variations within the receiver arrays [13]. The result of their research demonstrated that the errors due to variable element elevations were higher compared to errors due to disordered horizontal element positions.

Al-Shuhail and Al-Ghanim (2003) studied the performance of an array in the presence of near-surface heterogeneities. They used a model with two velocities (V_1 and V_2) [14]. They modeled the array performance using the velocity ratio $\left({}^{V_1}/_{V_2}\right)$ and number

of elements in V_1 and they found that the array performance generally increases with the number of elements in V_1. Similarly, the array performance decreased as the velocity ratio deviated. They noted that the worst case occurred only when one element is in layer 1 and $\left({}^{V_1}/_{V_2}\right)$ is minimum.

A response from the seismic array is described as the sum of outputs from an individual geophone of the array (Figure 1.1). The capability of a response from an array can be examined to attenuate undesired signals and capture the desired signals with reasonable distortion [15].

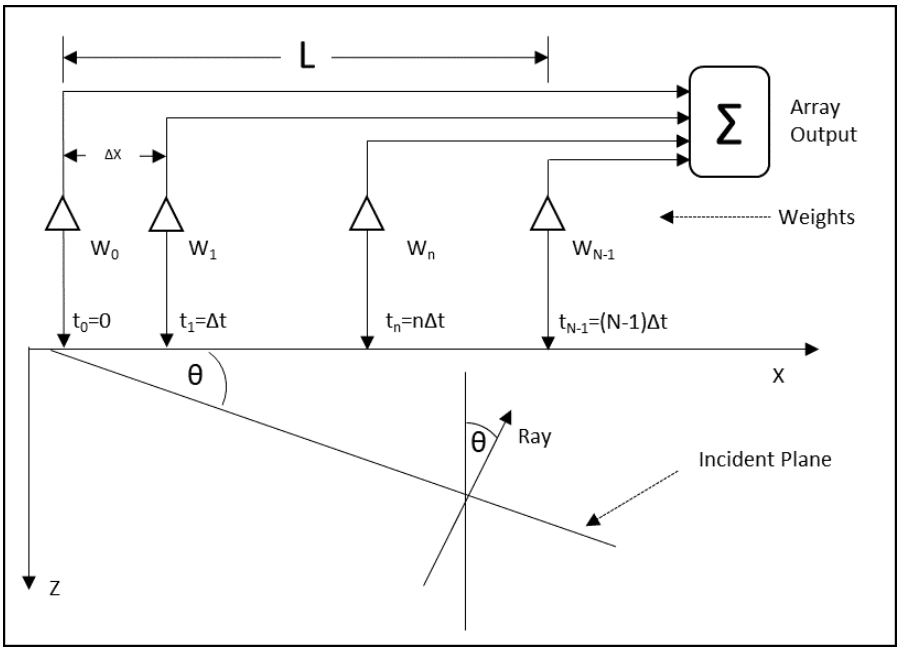

Figure *1*.**1.** A plane wave incident on the array at an angle θ. W_n indicates the weight of the nth geophone while t_n is the travel-time to the nth receiver. L represents the total length of the array and Δx is the geophone spacing. N is the number of receivers within the array (Al-Shuhail, 2011).

Akram (2007) studied the effect of array response in the presence of laterally varying thickness of the weathering layer. He generated several examples of the ideal impulse and Ricker wavelet responses of a 5-element equally weighted array shown in

Figure 1.2 [16]. He generated them for different values of impulse response length, which is defined as the total time across the array divided by the wavelet dominant period. In my study, the methodology of generating ideal impulse and Ricker wavelet response were similar to Akram (2007) work, however, the time delay between adjacent geophones was used instead of the impulse response length.

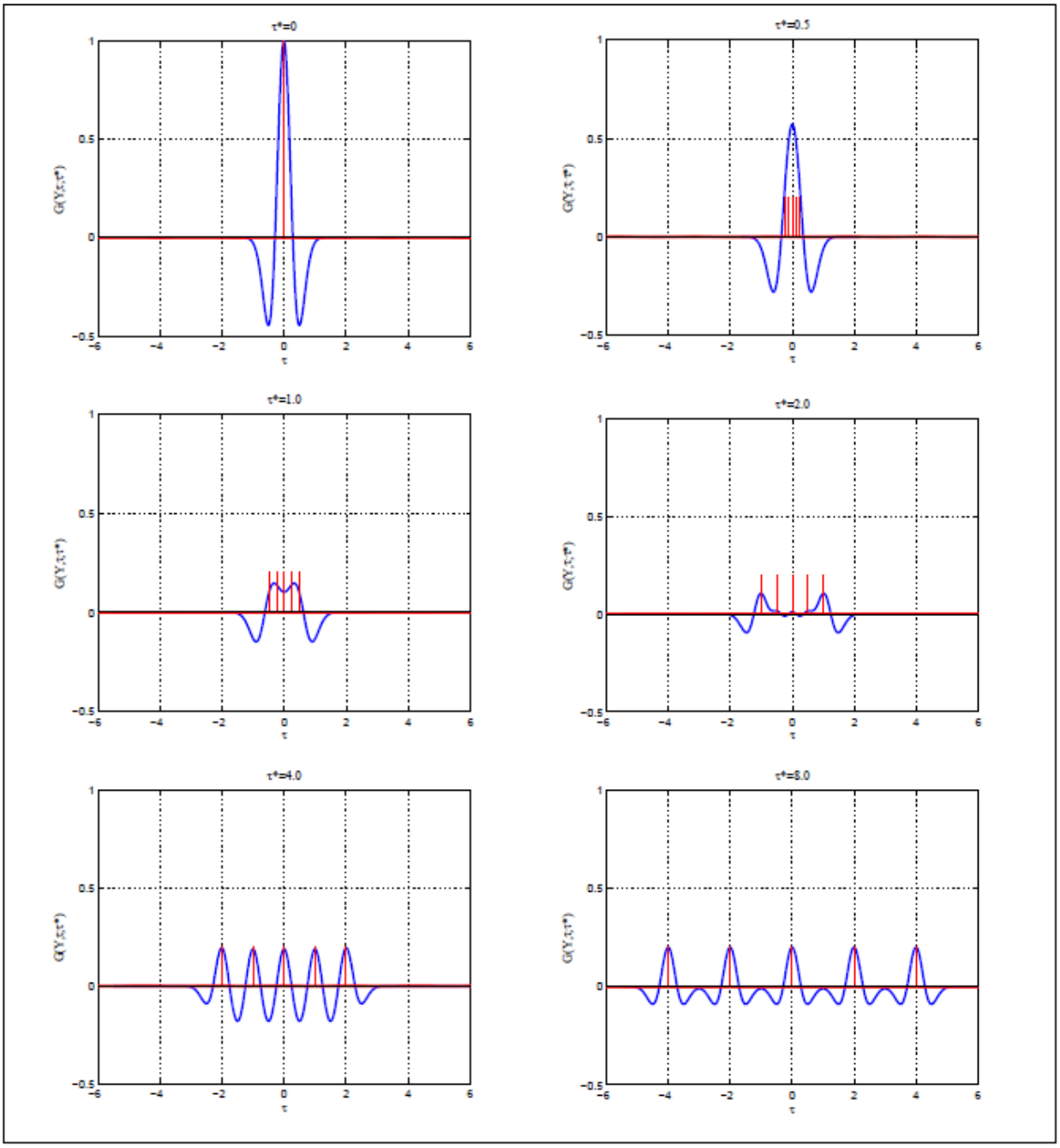

Figure 1.2. Impulse (red curve) and Ricker wavelet (blue curve) responses from a 5-element equally weighted array. $\mathbf{G}(\mathbf{Y}, \boldsymbol{\tau}; \boldsymbol{\tau}^*)$ is the array response. $\boldsymbol{\tau}^*$indicates array's impulse response length (Akram, 2007).

1.2. Problem statement and objective of the present study

As stated in the beginning of Chapter 1, the main purpose of ideal receiver arrays is to enhance the signal-to-noise ratio (S/N). Seismic acquisition will produce optimum S/N if the elements are planted on a flat surface and the precise spacing between elements is maintained. However, such location with precisely flat surface does not exist. Some locations have rugged topography or obstacles such as trees or houses, which require the elements to be planted on different elevations and positions between each of them (Figure 1.3).

In the previous section, there is an explanation regarding the previous studies which analyzed the array response using time-harmonic wave as an incident wave and the advantage of using impulsive signal instead of a time-harmonic wave. In addition, there were studies investigated the effects of elements position and elevation errors using impulsive signals, separately. However, the combined effects of variable element positions and elevations on the receiver seismic arrays response using impulsive signals have not been previously addressed.

Therefore, this study aims to quantify the degradation in the wavelet response of a seismic array caused by the combination of elements' position and elevation errors. The impulsive signal was used as an incident wavelet. In addition, weight variations were added into this study to make it as close as possible to the real condition. This study also aims to understand the application of the methodology on real data. The results of this study may benefit seismic contractors or oil and gas companies who are planning to do a seismic acquisition.

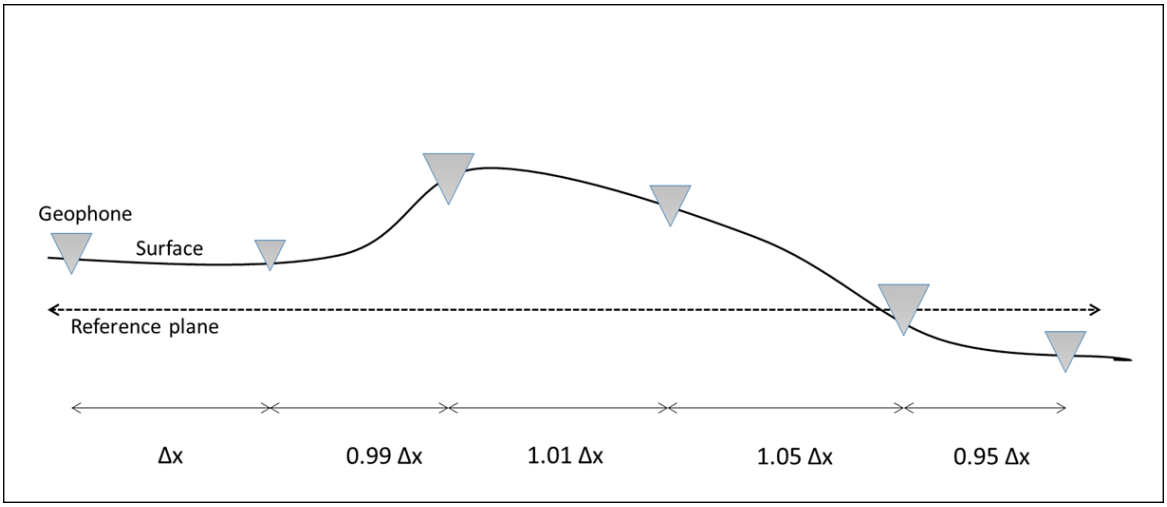

Figure *1*.**3.** Illustration of geophones planted in non-ideal condition. Geophones are planted in the undulated surface. Δ*x* represents the ideal distance between geophones and size of the triangle represents the weight of geophone.

1.3. Thesis structure

This thesis consists of six chapters. Chapter 1 contains the introduction of this study, including the literature used throughout this research. The literature review comprises the previous studies related to seismic array response, especially the studies which used impulse signals as incident wave. The reasons and the objectives of this study were explained in this chapter. Chapter 2 explains the methodology used to generate the wavelet array responses and to calculate the trace energies. It covers the generation of Ricker wavelet, impulse response, and the parameters applied to obtain the results. In the end of this chapter, the trace energy of ideal array response was presented. Chapter 3 provides the methodology used to generate the wavelet array response with errors. It also presents the equation of wavelet response used in this study by compiling the equations used in the previous studies. The results of this study are discussed in Chapter 4. The results consist of seven parts, corresponding to possible combinations of errors. The application

on seismic real data is presented in details in Chapter 5. It contains the calculation of the trace energy on real data, the process to obtain the parameters as well as applying the parameters on synthetic data. In the end, both results were compared. Conclusions and recommendations of the study are presented in chapter 6.

CHAPTER 2

METHODOLOGY

The purpose of this research is to assess the effects of combined errors in elevation, position, and weight of the elements within the array on the array response. To achieve this objective, the following methodology was used:

a) Generating the ideal impulse and wavelet responses

b) Calculating the trace energy of the ideal wavelet response

c) Generating the errors in elements' positions, elevations, and weights then applying them to generate the perturbed-array wavelet response

d) Calculating the trace energy of the perturbed-array wavelet response

e) Analyzing the percentage of error in the perturbed-array wavelet response

Details of my workflow are as follows:

2.1. Generating the ideal impulse and wavelet responses

The following parameters were used to generate the ideal impulse and wavelet response:

2.1.1. Number of elements

For practical reasons, I used only twelve elements within the linear arrays.

2.1.2. Weighting function

The equally weighted array is widely used because of the simplicity in its implementation and provides the necessary noise attenuation. An equally weighted 12-

element receiver array was utilized in this study, in which the weight associated with each individual receiver or n^{th} geophone (x_n) is:

$$W(\boldsymbol{x_n}) = \frac{\mathbf{1}}{\boldsymbol{N}} \tag{2.1}$$

where

N = total elements within the array

2.1.3. Wavelets

Al-Shuhail and Gangi, (1994) demonstrated that the wavelet array response from incident plane Ricker wavelets and Klauder wavelets are comparable. Thus, I used the zero-phase Ricker wavelet in this study. Moreover, a dominant frequency of 10 Hz and 2 millisec sampling interval were used as well.

Ricker (1953) made an early attempt to quantify the shape of the seismic wavelet in his classic paper, which described the wavelet shape that is now named after him [17]. The Ricker wavelet bears some resemblance to an actual physical seismic wavelet; however, it is actually the second derivative of the error function [18]. A Ricker wavelet (Figure 2.1) simulates the effect of an impulsive source such as a hammer or dynamite. The mathematical representation of the Ricker wavelet is given as:

$$\boldsymbol{R(t)} = \left[\mathbf{1} - \mathbf{2}\left(\boldsymbol{\pi f_p t}\right)^{\mathbf{2}}\right] \boldsymbol{e}^{-\left(\pi f_p t\right)^2} \tag{2.2}$$

where f_p is the dominant frequency of the wavelet [19]. As the wavelet carries several frequency components, there will be a dominant period, which can be defined with respect to the dominant frequency as:

$$T_p = \frac{2\sqrt{3/2}}{\pi f_p} = \frac{0.7797}{f_p} \tag{2.3}$$

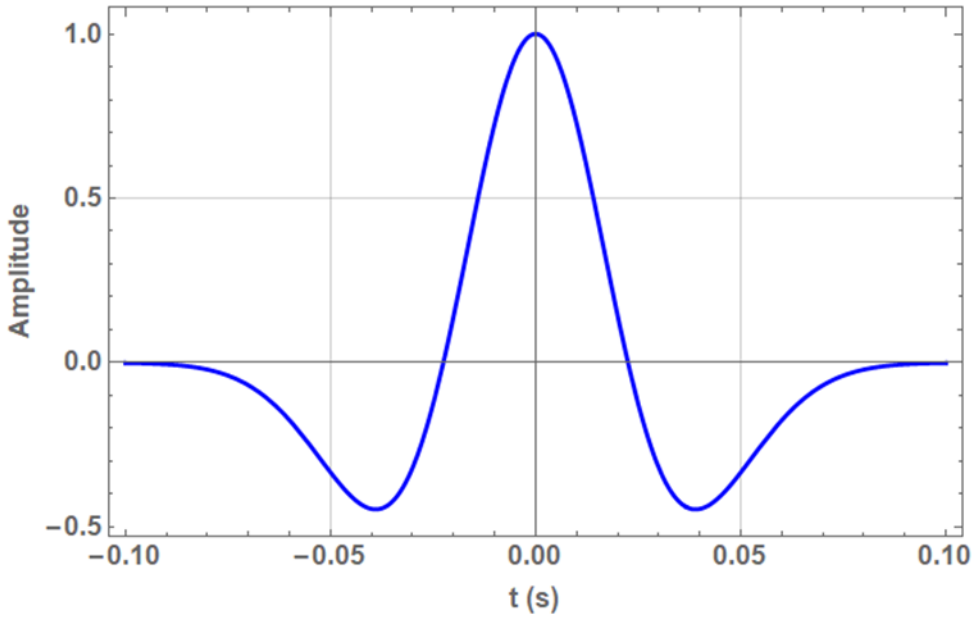

Figure *2*.**1.** Ricker wavelet of 10-Hz dominant frequency (f_p) and 0.078-s dominant period (T_p).

2.1.4. Generating the impulse and wavelet responses

The impulse response of the seismic array can be written as:

$$I(t) = \sum_{n=0}^{N-1} W(x_n)\delta(t - x_n n\Delta t) \tag{2.4}$$

where $\delta(t)$ indicates the delta (spike) function centered at t=0.

Moreover, the array wavelet response is the convolution between the impulse response and the Ricker wavelet:

$$\boldsymbol{G(t) = I(t) * R(t)}$$

(2.5)

and it can be written as:

$$\boldsymbol{G(t) = \sum_{n=0}^{N-1} W(x_n) R(t - x_n n \Delta t)}$$

(2.6)

where Δt is the time delay between adjacent geophones and N is the number of geophones in the array. Figure 2.2 illustrates the ideal wavelet responses of equally weighted 12-elements array and located on a flat surface with precise positions.

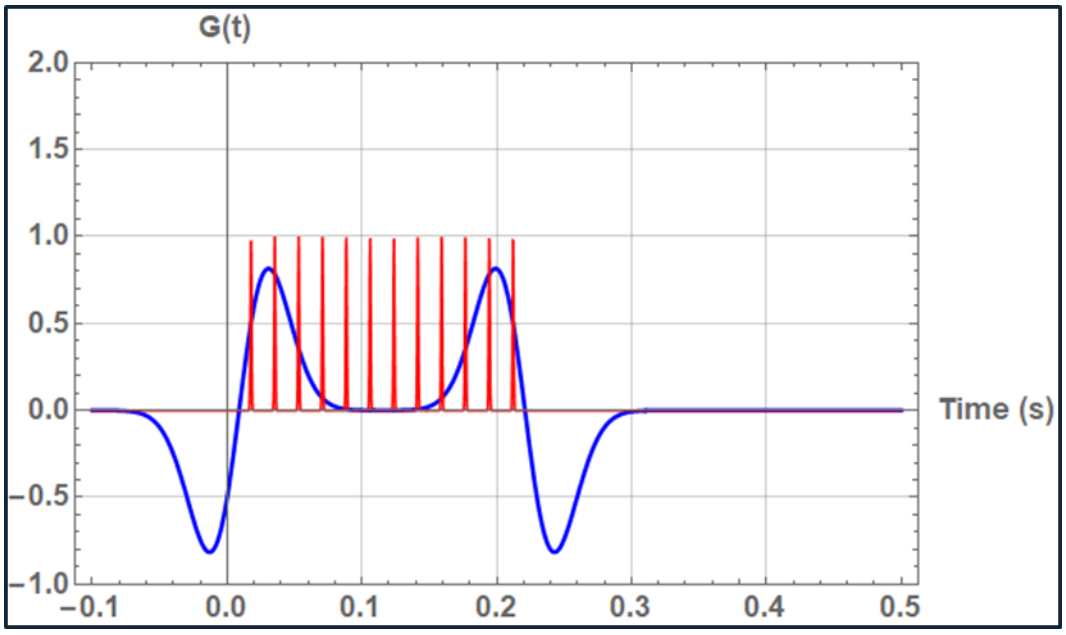

Figure 2.2. Ideal wavelet response to a Ricker wavelet of 10-Hz dominant frequency.

2.2. Calculating the trace energy of ideal wavelet response

To investigate the effects of combined errors in array response, trace energy was used to perform quantitative comparison between the ideal and perturbed array responses.

Trace energy, which is defined as the sum of the squared amplitudes of the array response, can be shown as:

$$\boldsymbol{E(t) = \sum_{m=1}^{M} G^2(t)}$$

(2.7)

where ***G(t)*** is the wavelet response of the array and *M* is the number of samples in ***G(t)***. To simplify the comparison, the trace energy was normalized by using the equation below:

$$\boldsymbol{E_n = \frac{E(t)}{E(t = 0)}}$$

(2.8)

where *E(t = 0)* = 2,154.3 represents the case when all wavelets were centered at *t* = 0 and add up in phase.

Furthermore, in decibel (dB) scale, the normalized trace energy is:

$$\boldsymbol{E_n' = 20 \log_{10} E_n} \text{ (dB)}$$

(2.9)

Due to variations in incidence angle and element's spacing, the trace energy of ideal array response was plotted in the three-dimensional surface (Figure 2.3). However, to simplify the comparison between the results of this study, the angle of incidence (θ) has been fixed. The value of θ throughout this study was $45°$ and it was illustrated in a two-dimensional curve (Figure 2.4).

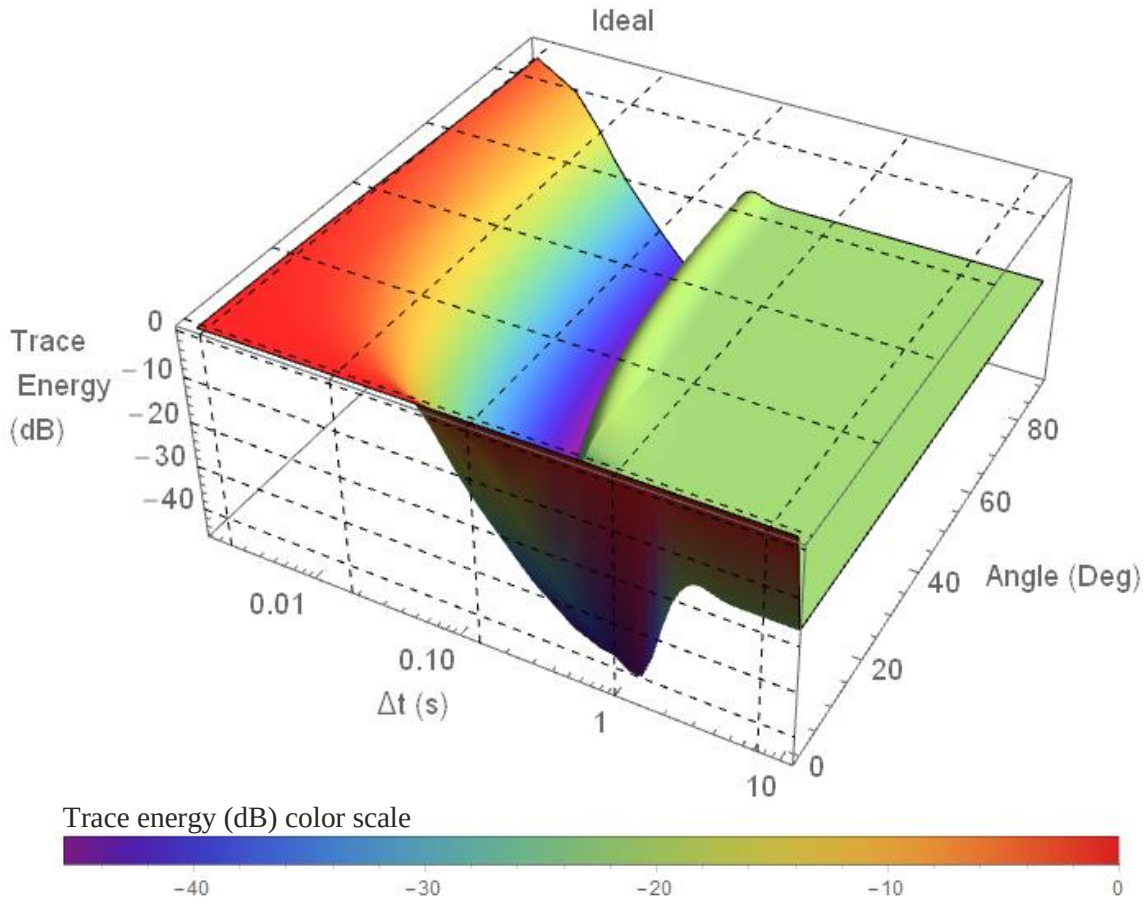

Figure 2.3. A three-dimensional surface represents the trace energy of an ideal array response with various incidence angles (θ = 0º - 90º).

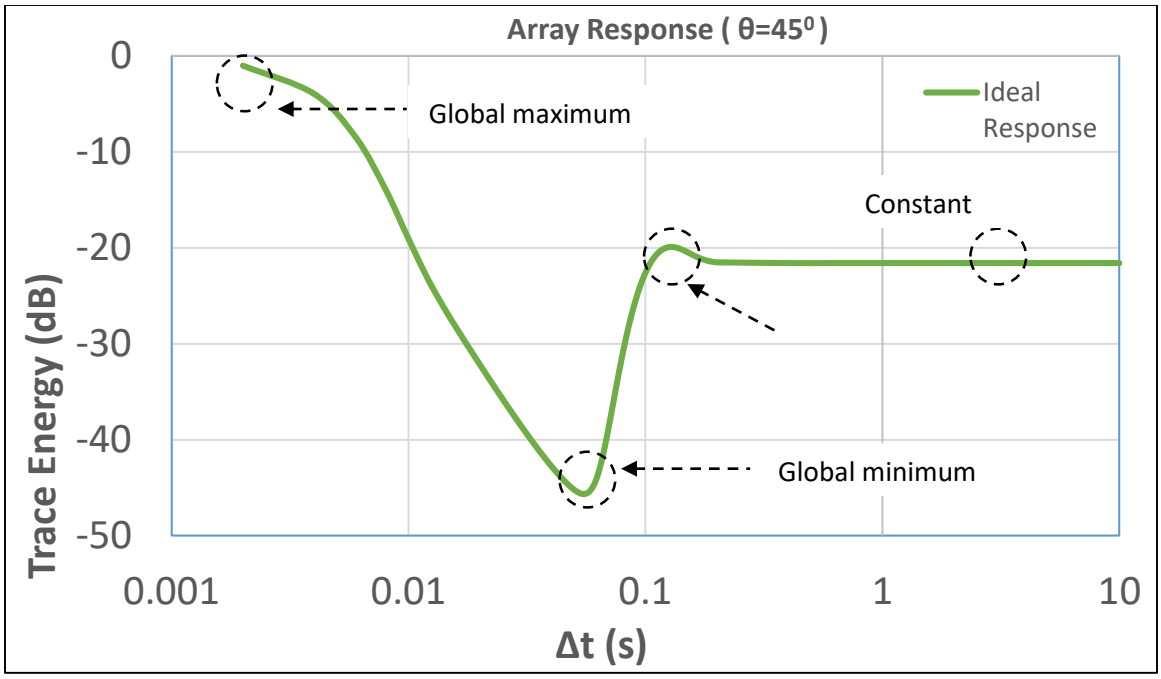

Figure *2*.**4.** Trace energy of ideal array response with fixed incidence angle (θ=45°).

Figure 2.4 illustrates the trace energy of an ideal array response at 45º incidence angle. Four interesting points were illustrated in the figure: the global maximum, global minimum, local maximum, and flat part of the curve. The global maximum point appears when the wavelets have perfect constructive interference (at $\Delta t = 0$) making *G(t)* maximum (Figure 2.5a). The wavelets have maximum destructive interference (at Δt = 0.054 s) making *G(t)* minimum (Figure 2.5b) at the global minimum point. The wavelets have partial constructive interference at Δt =0.128 s (Figure 2.5c) producing the local maximum point. Finally, the wavelets were completely separated beyond this point resulting in the amplitudes of a single wavelet (Figure 2.5d). The global minimum point was used in Chapter 4 to compare the results.

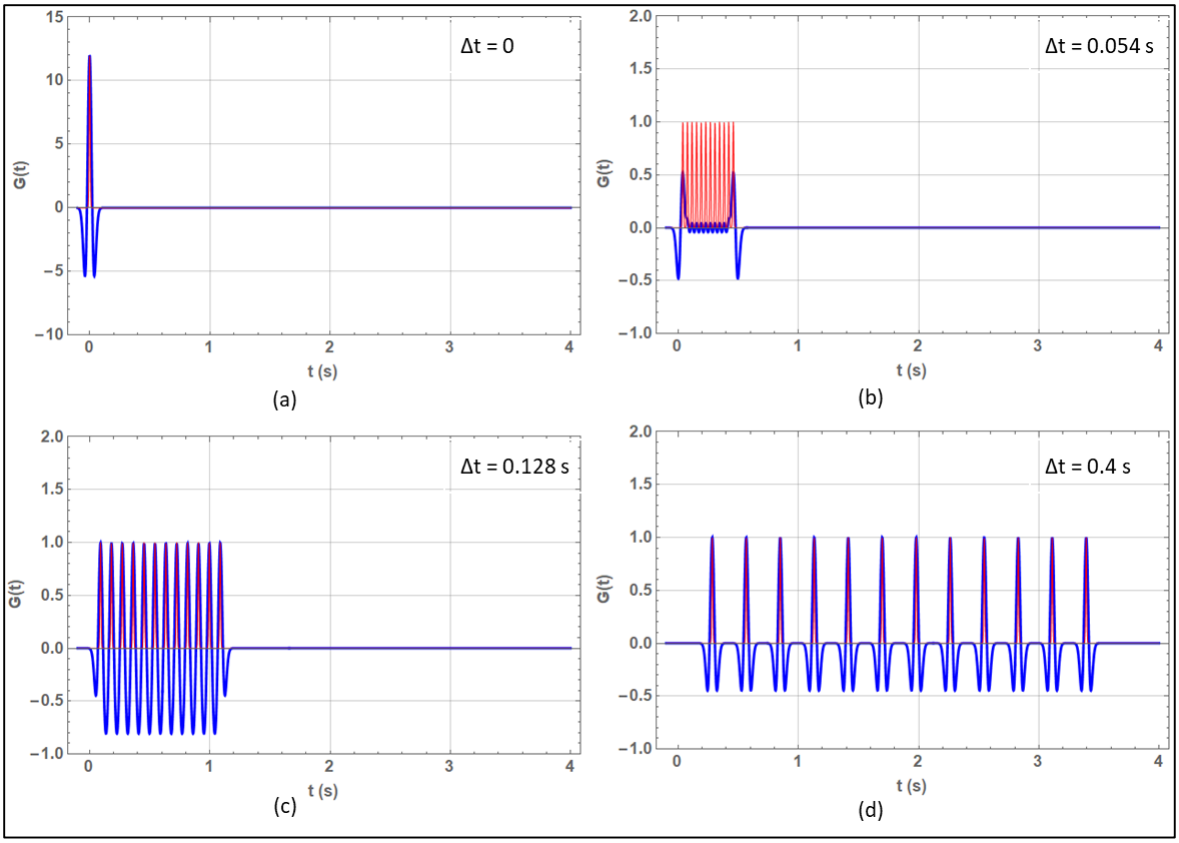

Figure *2*.**5.** Impulse response *I(t)* shown by red spikes and Ricker wavelet responses *G(t)* shown by blue curves, for an equally weighted 12-element array for (a) Global maximum at Δt = 0, (b) Global minimum at Δt = 0.054 s, (c) Local maximum at Δt = 0.128 s, and (d) Constant response at Δt = 0.4 s.

CHAPTER 3

THE ARRAY WAVELET RESPONSE WITH ERRORS IN ELEMENTS' POSITIONS, ELEVATIONS, AND WEIGHTS

In the present study, I investigated the effect of elevation and position errors in the elements of the array wavelet responses. In this case, the errors represent the actual elevation and position of the geophones. Both errors are possible due to obstacles along the seismic acquisition area. In addition, I also investigated the effect of errors on the weight of elements. The workflow below was used to apply the errors into the array response:

1) Generate error distributions that simulate the distribution of typical seismic noise.
2) Apply these errors to the array impulse response to simulate the effect of errors on the elements' elevations, positions, and weights.
3) Generate array wavelet response with errors by convolving the array impulse response with errors, as mentioned in step (2), with the incident wavelet.
4) Analyze the resulting wavelet responses using their normalized trace energies.

3.1. Generating the errors

Sax (1968) stated that most types of seismic noise encountered in the field can be represented by stationary, random, zero-mean Gaussian distributions [20]. Gaussians distributions or normal distributions are important in statistic and are often used in natural or social sciences to represent real-valued random variables whose distributions are not known. The errors in the elements' weights, positions, and elevations are considered as types of seismic noise, thus stationary, random, zero-mean Gaussian distributions were used to represent such errors. After the generation of zero-mean, unity-standard deviation

Gaussian distribution, the members of the distribution were multiplied by a factor σ to transform the distribution to one with the appropriate standard deviation (σ). The standard deviations (σ) of the elements' weights, positions, and elevations used in this study were 10% and 20%.

3.2. Generating impulse responses with errors in elements' position, elevations, and weights

To produce the array impulse response with errors, *N* members belonging to a Gaussian distribution with zero mean and σ standard deviation were generated and were applied to the elements' weights, elevations, and positions, where *N* is the number of elements in the array. This procedure was done for 150 values of Δt or the elements' spacing in time. The elements' spacing in time was calculated by dividing the elements' spacing (Δx) by a constant near-surface velocity (v=*500 m/s*). The elements' spacing (Δx) varied from 0 to 5,000 *m*. It had a 1-*m* interval between 0 to 100 *m* and 100-*m* interval between 100 *m* to 5,000 *m*. To obtain statistically significant results, the process of was repeated 32 times for each standard deviation and their average response was used in subsequent procedure.

Benson (1989) introduced the normalized arrival time of the n^{th} geophone of the array (τ_{en}) [21], which results of the application of an error in element's position (Ex_n) as indicated below:

$$\boldsymbol{\tau_{en} = (n + Ex_n) \sin \theta \, \Delta \tau},$$

(3.1)

where n = 0, 1, 2, …, N-1.

Furthermore, Al-Shuhail (1993) explained the travel-time to the n^{th} geophone including the effect of elevation as:

$$\boldsymbol{\tau_{en}(\theta) = (n \sin \theta + Ez_n \cos \theta)\Delta\tau},$$

(3.2)

where Ez_n represents the error in elevation of the n^{th} geophone of the array obtained from a zero-mean, σ-standard deviation, Gaussian distribution [22].

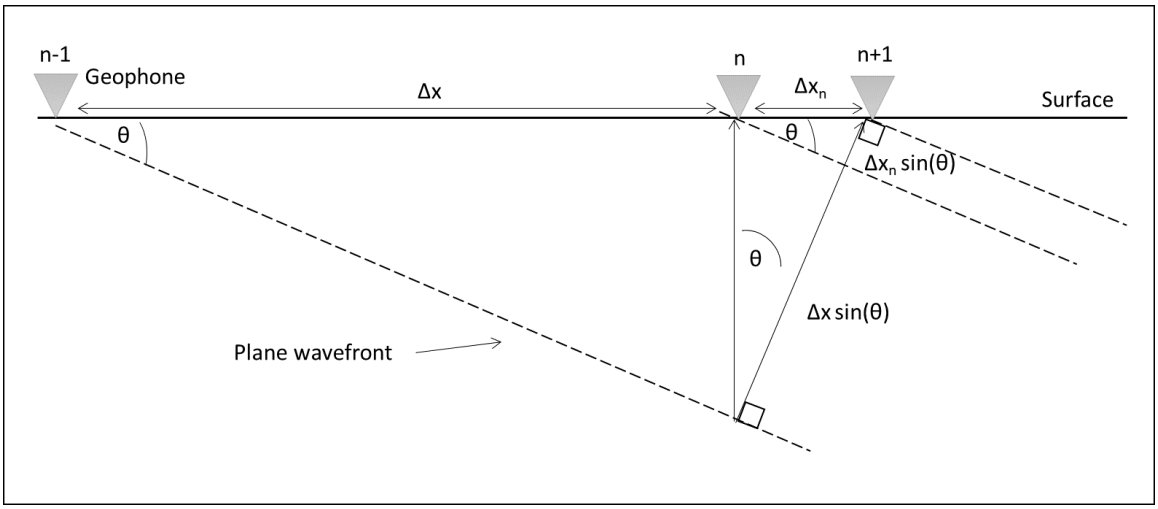

Figure *3*.**1.** Illustration of error in element's position.

In both cases, the errors in elements' positions (Ex_n) and elevations (Ez_n) were calculated with respect to the elements' spacing (Δx), which variable that can be controlled.

$$\boldsymbol{Ex_n = {\Delta x_n}/{\Delta x}}$$

(3.3)

$$\boldsymbol{Ez_n = {z_n}/{\Delta x}}$$

(3.4)

The term $\Delta\tau$ in equations (3.1) and (3.2) is:

$$\Delta\boldsymbol{\tau} = {}^{\Delta\boldsymbol{x}}/_{(\boldsymbol{T_p v})},$$

(3.5)

where:

Δx = element's spacing, T_p = dominant period, v = velocity.

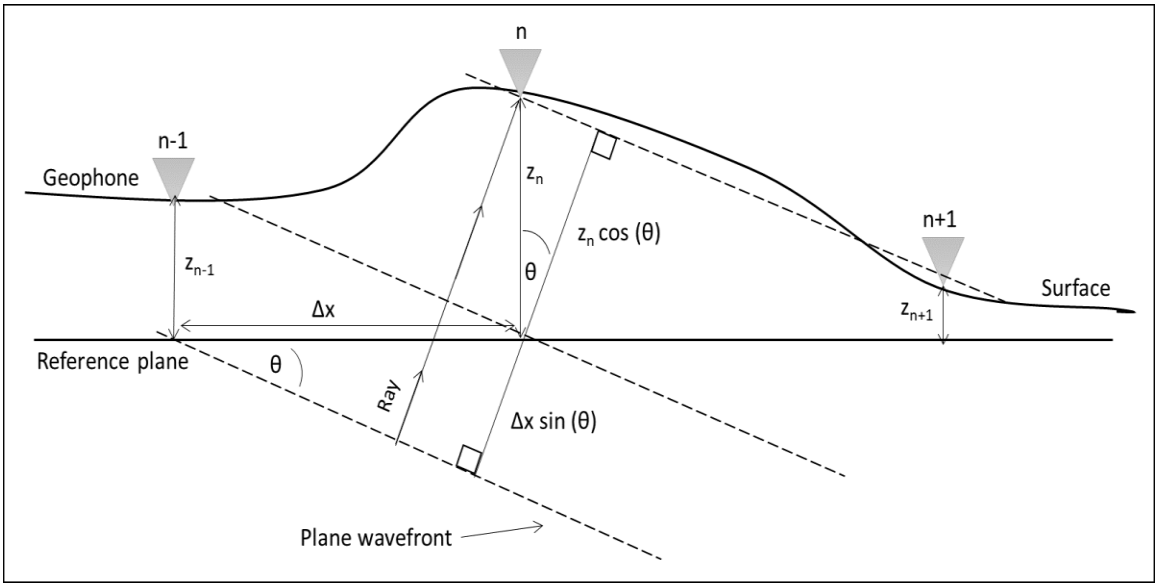

Figure *3.2.* Illustration of error in element's elevation.

3.3. Generating wavelet responses with errors in elements' position, elevations, and weights

The wavelet responses with errors were generated by convolving the impulse response with errors with the Ricker wavelet using equation (2.6). This results in the following equation:

$$\boldsymbol{G(t)} = \sum_{\boldsymbol{n=1}}^{\boldsymbol{N}} \left[(\mathbf{1} + \boldsymbol{Ew_n})\, \boldsymbol{R}\left[\boldsymbol{t} - \left(\frac{\boldsymbol{\Delta x}}{\boldsymbol{V}} \right) (\boldsymbol{n}\ \mathbf{sin}(\boldsymbol{\theta}) + \boldsymbol{Ex_n}\ \mathbf{sin}(\boldsymbol{\theta}) + \boldsymbol{Ez_n}\ \mathbf{cos}(\boldsymbol{\theta})) \right] \right]$$

(3.6)

where Ew_n represents the error in weight of the n^{th} geophone of the array obtained from a zero-mean, σ-standard deviation, Gaussian distribution.

CHAPTER 4

RESULTS ON THE APPLICATION OF SYNTHETIC DATA

Using the methods and procedures described in Chapters 2 and 3, I obtained the results outlined in the following section. Every section consists of three figures. The two three-dimensional surface figures represent the average of 32 array wavelet responses of an equally weighted 12-element array, with 10% and 20% standard deviation errors. Both figures were generated using incidence angles between θ=0° to 90° and element spacing between Δt= 0 s to 10 s plotted on log scales. The third figure is a two-dimensional figure comparing the trace energies between the ideal array and perturbed array response at 45° incidence angle. There will be quantitative estimation for each case of the amount of error producing acceptable degradation of trace energy. I considered 10% degradation of trace energy acceptable.

4.1. Trace energy of the array response with errors in the elements' position.

Figures 4.1, 4.2, and 4.3 show the trace energies from array response affected by elements' position error. Figures 4.1 and 4.2 show three-dimensional surfaces, which represent trace energy of perturbed array response affected by 10% and 20% standard deviation errors in the elements' position, respectively. The differences between ideal array and perturbed array response affected by elements' position error were difficult to distinguish in the three-dimensional figure. On the other hand, the comparison more unambiguous when two-dimensional curves were used (Figure 4.3). The degradation of the perturbed array response can be differentiated by looking at a global minimum in the curve. The ideal curve reached minimum trace energy at -45.6 dB at Δt = 0.054 s as 10% standard

deviation errors in element's position were added and led to the degradation of 13% minimum trace energy; however, if 20% standard deviation errors were added to element's position, a 24% degradation of minimum trace energy occurred.

The degradation of trace energy will be more acceptable, which is less than 10% degradation if the error in elements' position is less than 7% from the ideal condition.

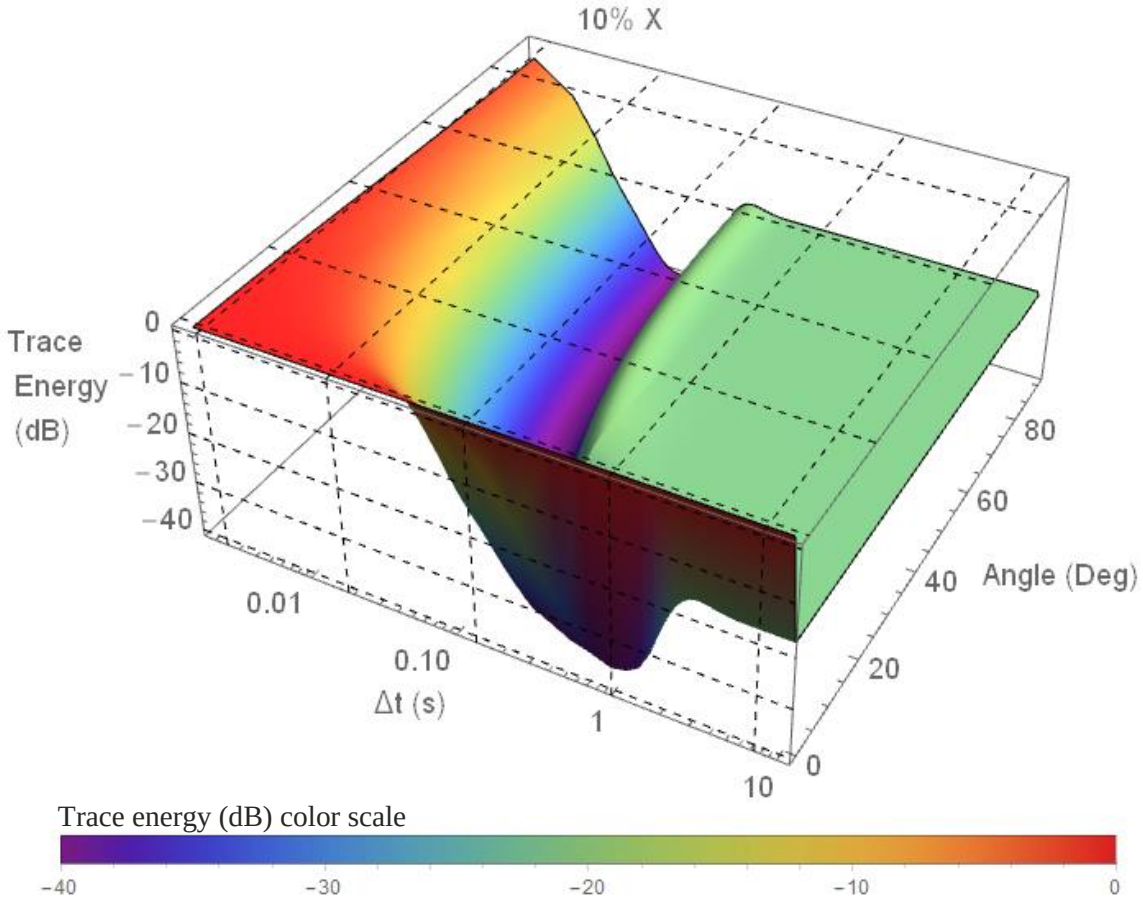

Figure *4.1.* A three-dimensional surface representing the trace energy of perturbed array response affected by 10% standard deviation errors in elements' position with various incidence angles (θ=0º - 90º).

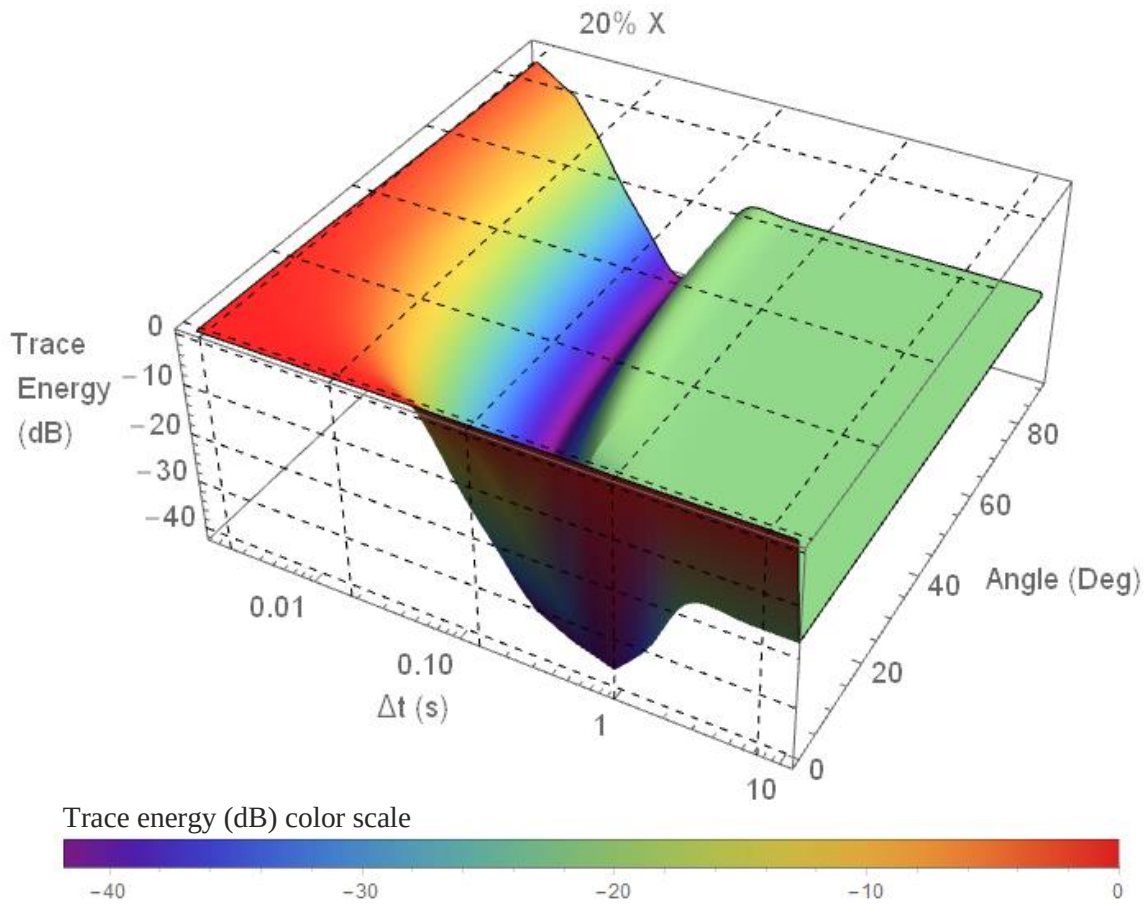

Figure *4*.**2.** A three-dimensional surface representing the trace energy of perturbed array response affected by 20% standard deviation errors in elements' position with various incidence angles (θ=0º - 90º).

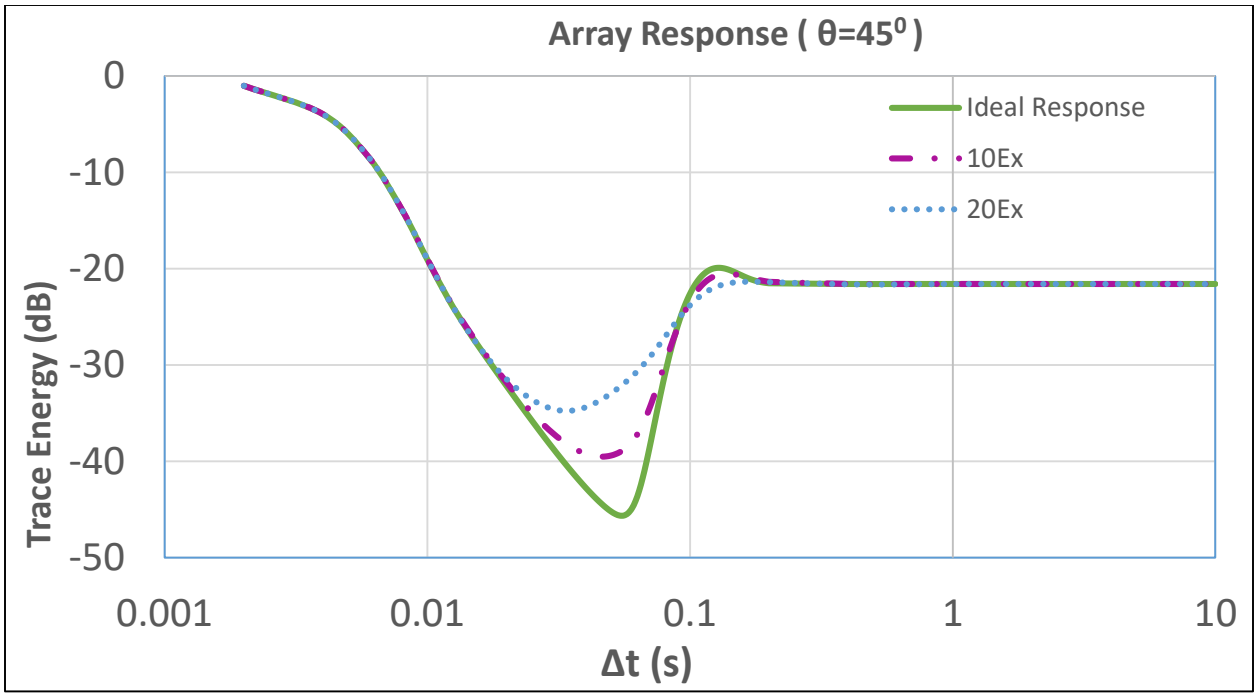

Figure *4.3.* Comparison between the ideal array and perturbed array responses with 10% and 20% standard deviation errors in elements' position.

4.2. Trace energy of the array response with errors in the elements' elevation.

Figures 4.4, 4.5, and 4.6 show the trace energy of the array response affected by elements' elevation error. Figures 4.4 and 4.5 show three-dimensional surfaces that represent trace energy of perturbed array response affected by 10% and 20% standard deviation errors in the elements' elevation, respectively. The degradation of perturbed array response appeared in small incidence angle, however, it did not occur in perturbed array response affected by elements' position.

As seen in the two-dimensional curves or Figure 4.6, the minimum trace energy degraded up to 13% on the addition of 10% standard deviation error in elements' elevation. Increasing standard deviation errors to 20% caused a 23% degradation in minimum trace energy.

The degradation of trace energy caused by the error in element's elevation is comparable to that in element's position. The addition of 7% standard deviation error in element's elevation will make the trace energy degradation tolerable (less than 10%).

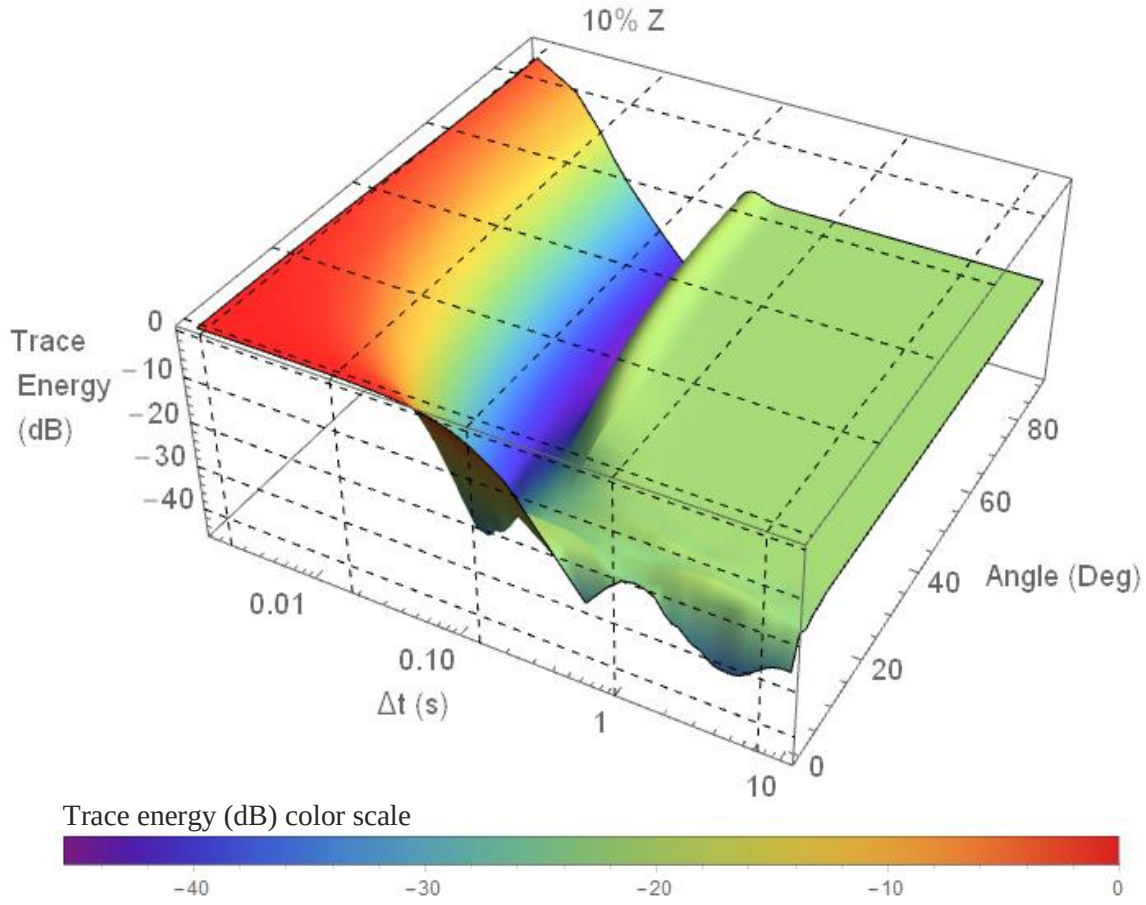

Figure 4.4. A three-dimensional surface representing the trace energy of perturbed array response affected by 10% standard deviation errors in elements' elevation with various incidence angles (θ=0º - 90º).

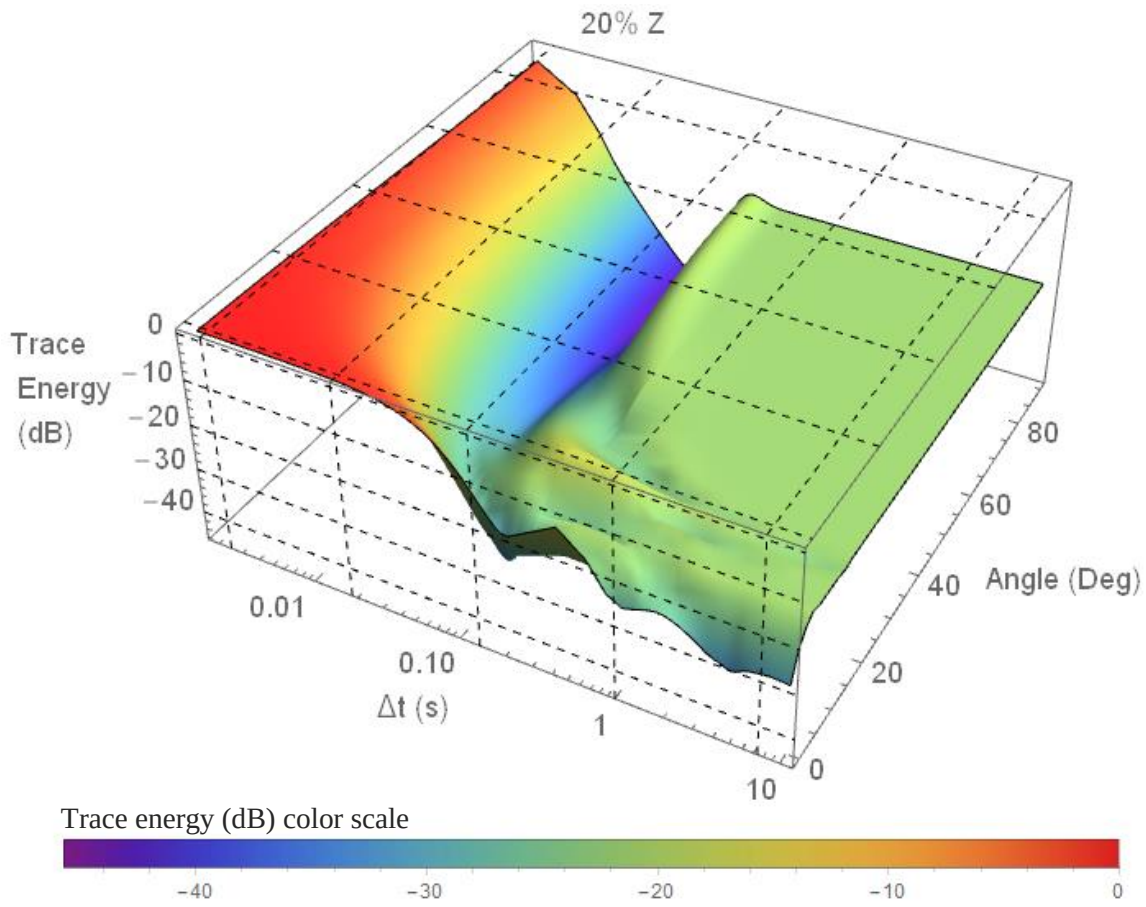

Figure *4*.**5.** A three-dimensional surface representing the trace energy of perturbed array response affected by 20% standard deviation errors in elements' elevation with various incidence angles (θ=0º - 90º).

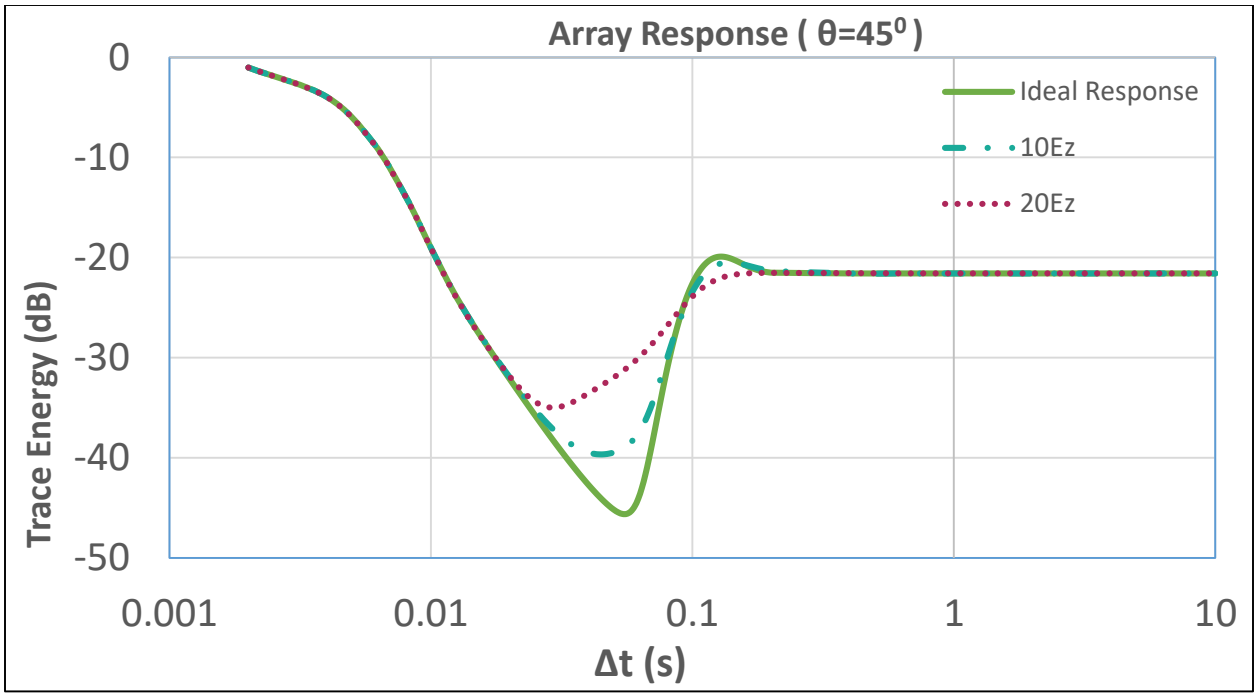

Figure *4.***6.** Comparison between the ideal array and perturbed array responses with 10% and 20% standard deviation errors in elements' elevation.

4.3. Trace energy of the array response with errors in the elements' weights.

Figures 4.7, 4.8, and 4.9 show the trace energy of the array response affected by elements' weight error. Figures 4.7 and 4.8 show three-dimensional surfaces, which represent trace energy of perturbed array response affected by 10% and 20% standard deviation errors in the elements' weight, respectively. The degradation of perturbed array response is hard to distinguish in three-dimensional surfaces and two-dimensional curves. As seen in Figure 4.9, in the small degradation in two-dimensional curves, the minimum trace energy degraded by only 2% on the addition of 10% standard deviation error in elements' weight. Addition of standard deviation errors up to 20% led to only 6% degradation of minimum trace energy.

The degradation of trace energy caused by the error in element's weight is acceptable even with 20% standard deviation errors.

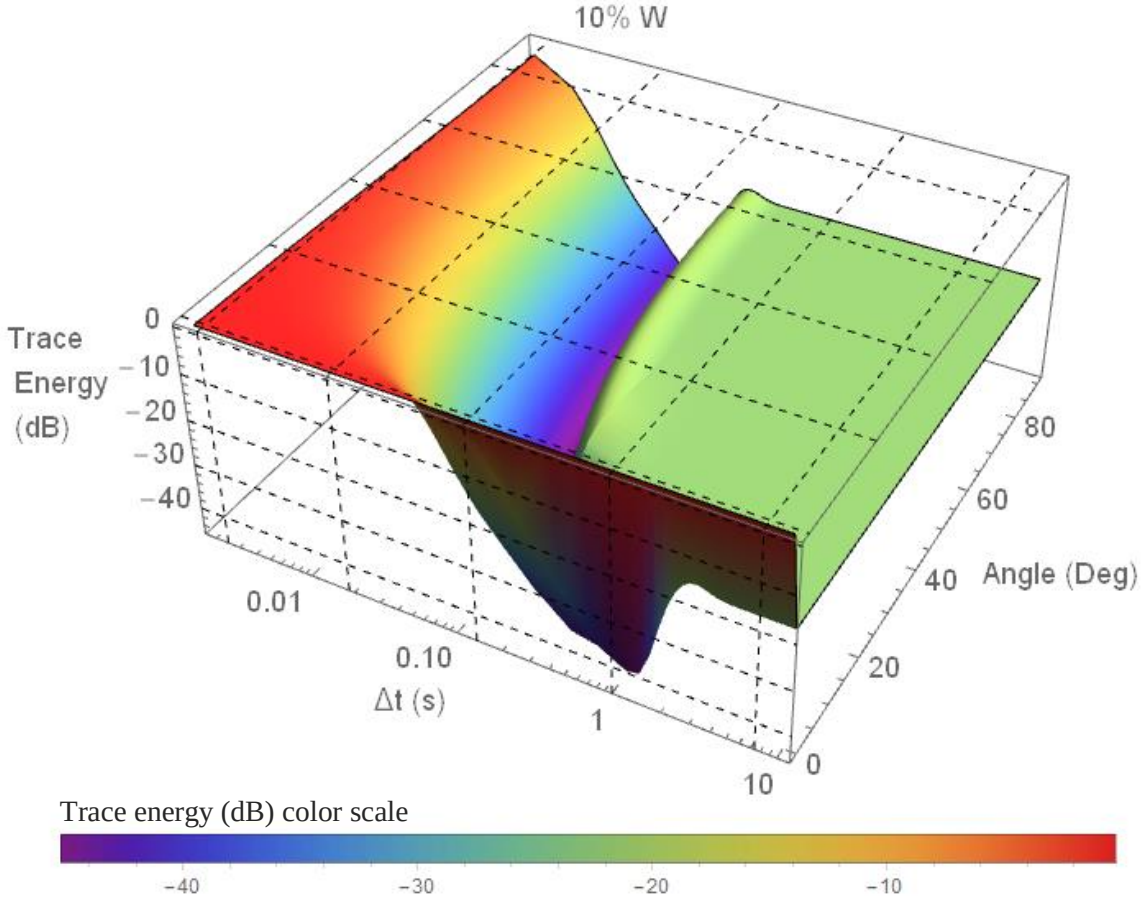

Figure *4.7.* A three-dimensional surface representing the trace energy of perturbed array response affected by 10% standard deviation errors in elements' weight with various incidence angles (θ=0º - 90º).

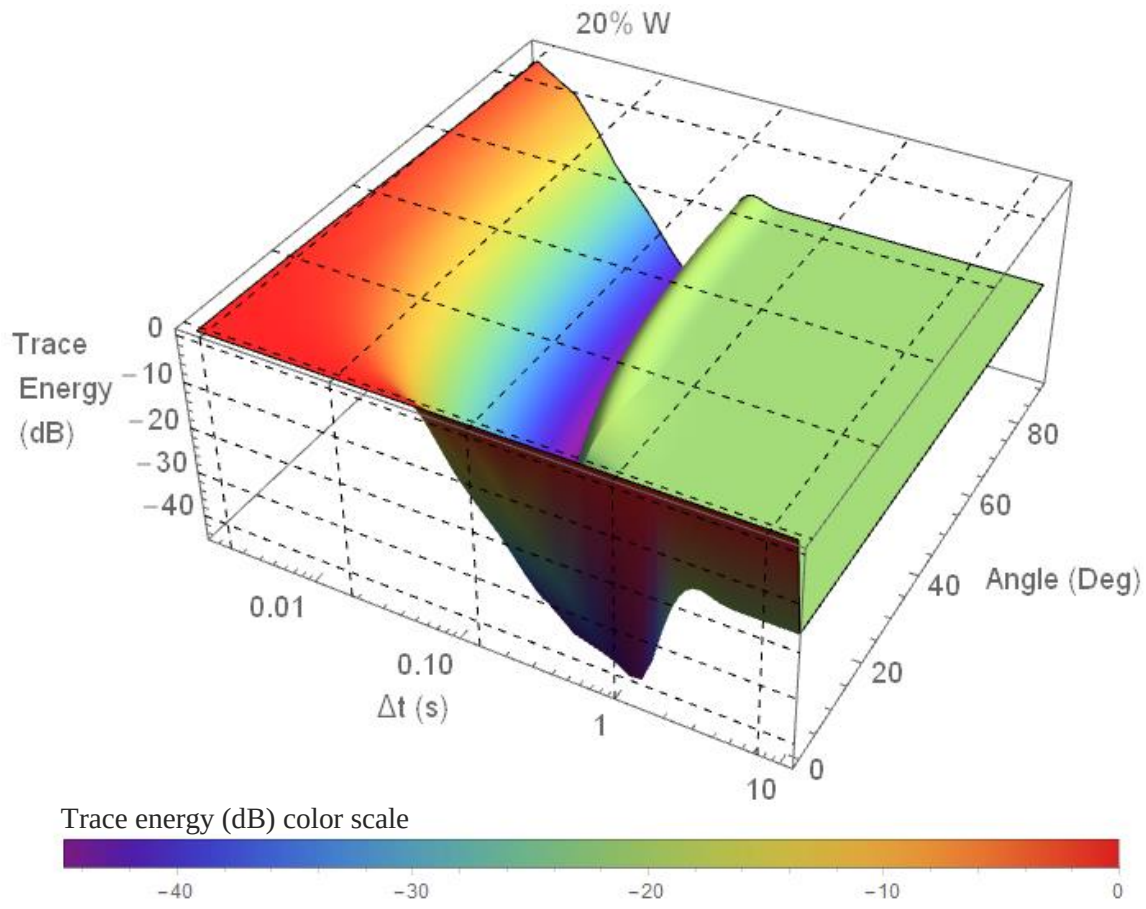

Figure 4.8. A three-dimensional surface representing the trace energy of perturbed array response affected by 20% standard deviation errors in elements' weight with various incidence angles (θ=0º - 90º).

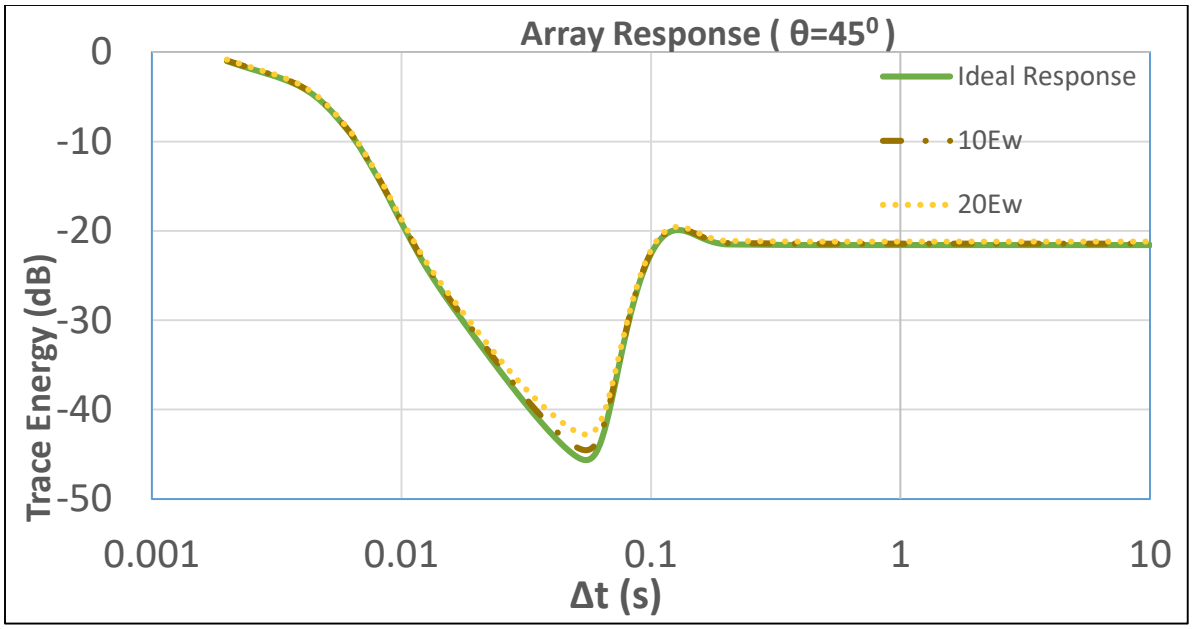

Figure *4*.**9.** Comparison between the ideal array and perturbed array responses with 10% and 20% standard deviation errors in elements' weight.

4.4. Trace energy of the array response with combined errors in the elements' position and elevation.

Figures 4.10, 4.11, and 4.12 show the trace energy of the array response affected by combined errors of elements' position and elevation. Figures 4.10 and 4.11 show three-dimensional surfaces, which represent trace energy of perturbed array response affected by 10% and 20% standard deviation errors in the elements' position and elevation, respectively. This response is comparable to the perturbed array response affected by the error in elements' elevation. The degradation of perturbed array response appeared in small incidence angle.

By observing the two-dimensional curves (Figure 4.12), the minimum trace energy of perturbed array responses caused by combined errors degraded at a greater degree as compared to that of a single error. However, it does not reflect the total of both

errors. The addition of 10% standard deviation error in each elements' position and elevation caused a 13% trace energy degradation. However, combining both errors could degrade the trace energy up to 17%. Moreover, there will be 28% trace energy degradation if 20% standard deviation in combined errors was used.

Since the degradation of trace energy is higher in this case as compared to the single error, it requires more accuracy when planting the elements. The degradation will be more acceptable, which is less than 10% degradation if each error is less than 3% from the ideal condition.

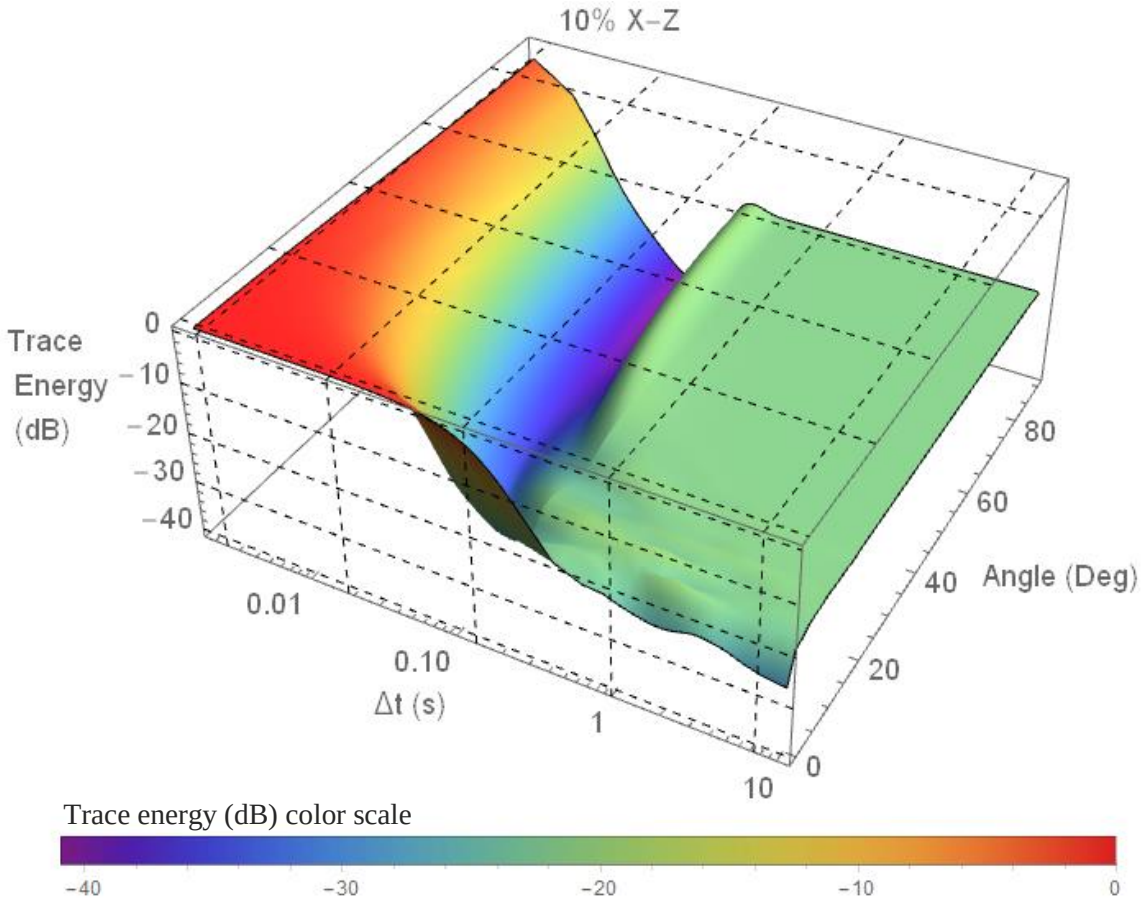

Figure 4.10. A three-dimensional surface representing the trace energy of perturbed array response affected by 10% standard deviation errors in elements' position and elevation with various incidence angles (θ=0º - 90º).

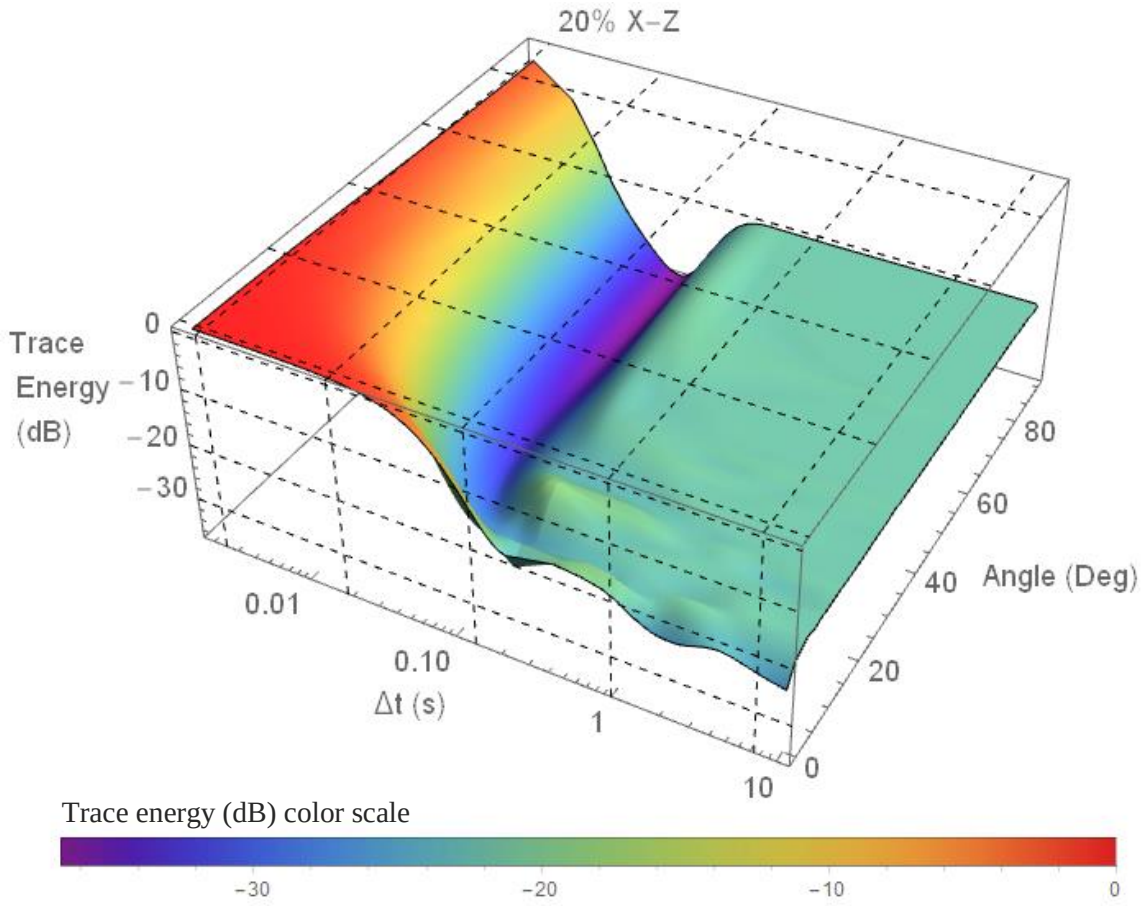

Figure 4.11. A three-dimensional surface representing the trace energy of perturbed array response affected by 20% standard deviation errors in elements' position and elevation with various incidence angles (θ=0º - 90º).

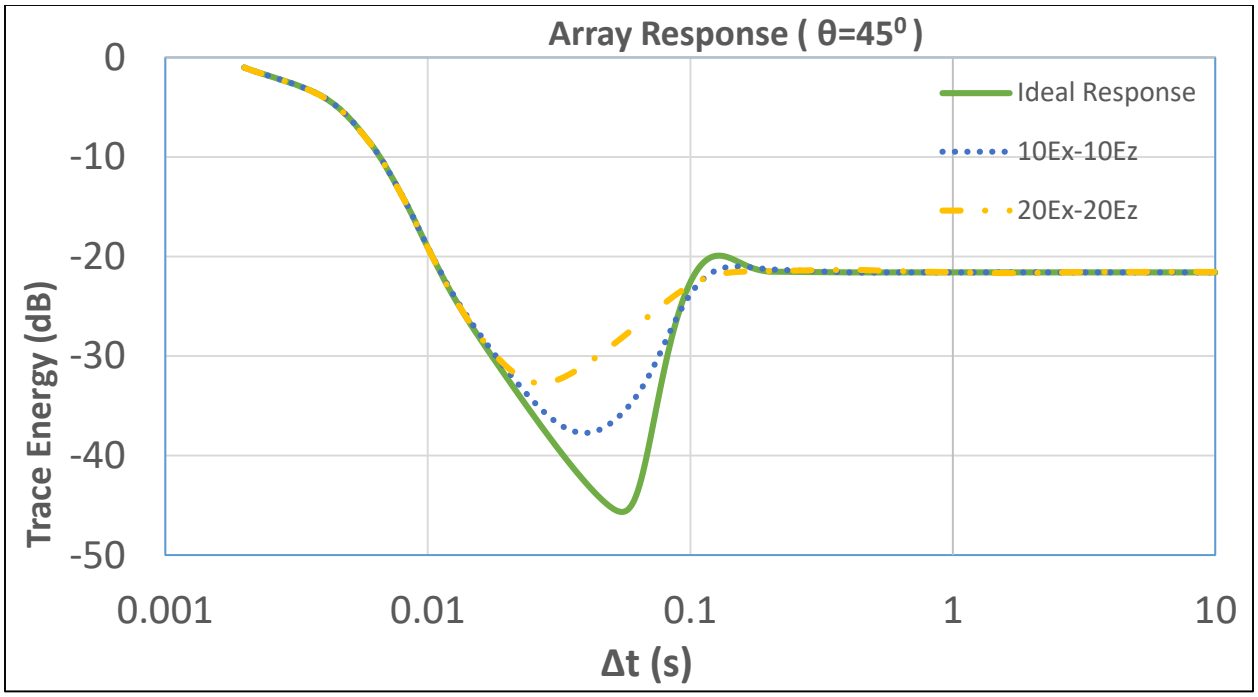

Figure *4*.**12.** Comparison between the ideal array and perturbed array responses with 10% and 20% standard deviation errors in elements' position and elevation.

4.5. Trace energy of the array response with combined errors in the elements' position and weights.

Figures 4.13, 4.14, and 4.15 demonstrate the trace energy of the array response affected by combined errors of elements' position and weight. Figures 4.13 and 4.14 present three-dimensional surfaces, which represent trace energy of perturbed array response affected by 10% and 20% standard deviation errors in the elements' position and weight, respectively. The differences between ideal array and perturbed array responses affected by combined elements' position and weight errors are difficult to distinguish in the three-dimensional figures. However, the comparison between the responses is clearer in the two-dimensional curves (Figure 4.15). The degradation of the perturbed array response can be determined by looking at a global minimum in the curve. The addition of

10% standard deviation combined errors of element's position and weight led to the degradation of 12% minimum trace energy, which is less than the combined errors of elements' position and elevation. Furthermore, the minimum trace energy degraded up to 26% on the addition of 20% standard deviation of combined errors.

This case has smaller degradation as compared to the case of combined effect of element's position and elevation error. Hence, this case only needs 9% error for each type to achieve acceptable trace energy.

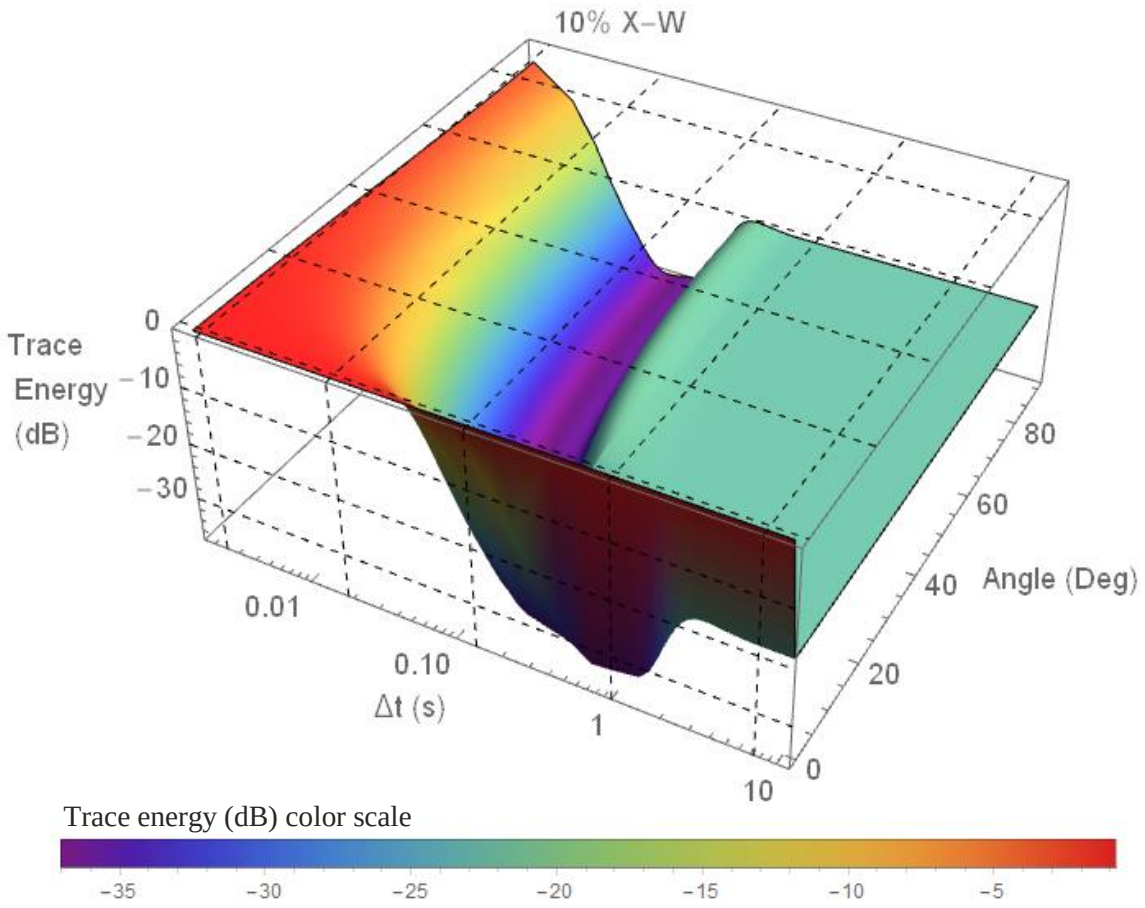

Figure *4*.13. A three-dimensional surface representing the trace energy of perturbed array response affected by 10% standard deviation errors in elements' position and weight with various incidence angles (θ=0º - 90º).

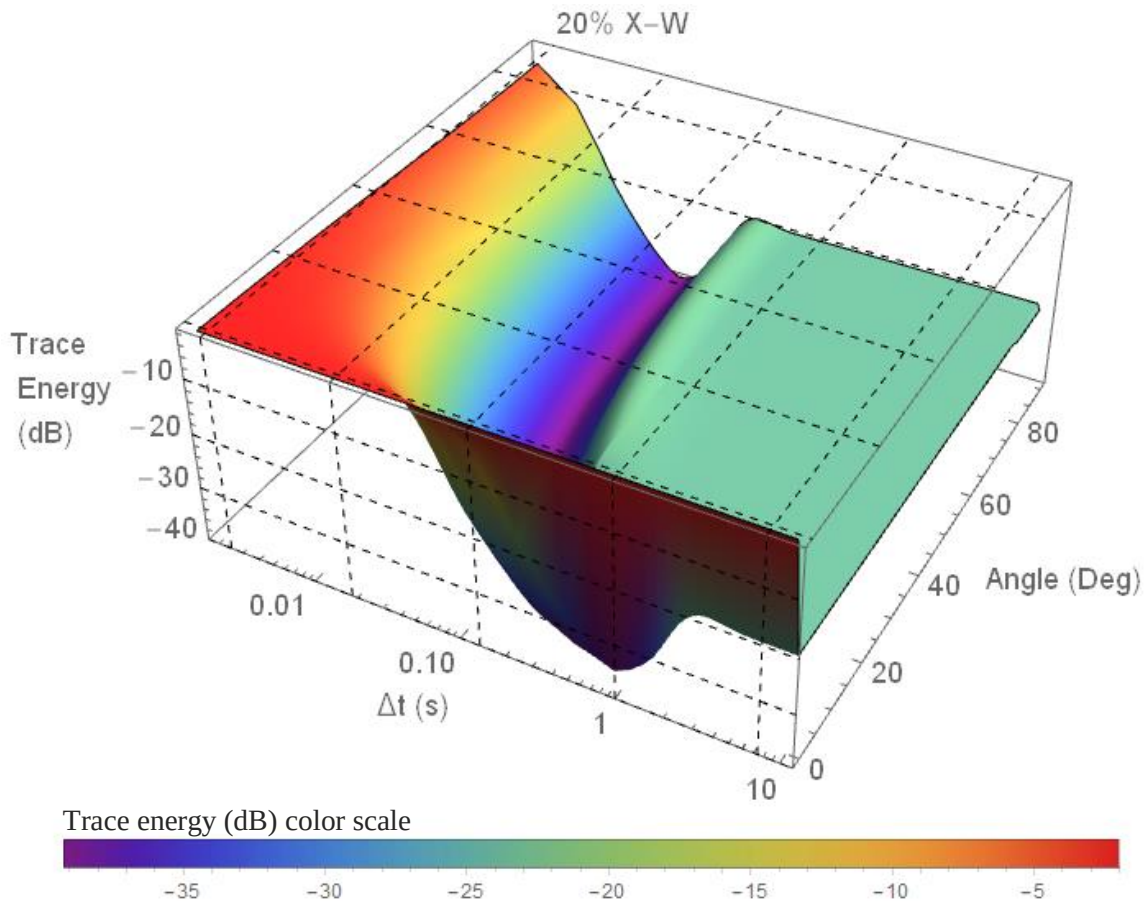

Figure 4.14. A three-dimensional surface representing the trace energy of perturbed array response affected by 20% standard deviation errors in elements' position and weight with various incidence angles (θ=0º - 90º).

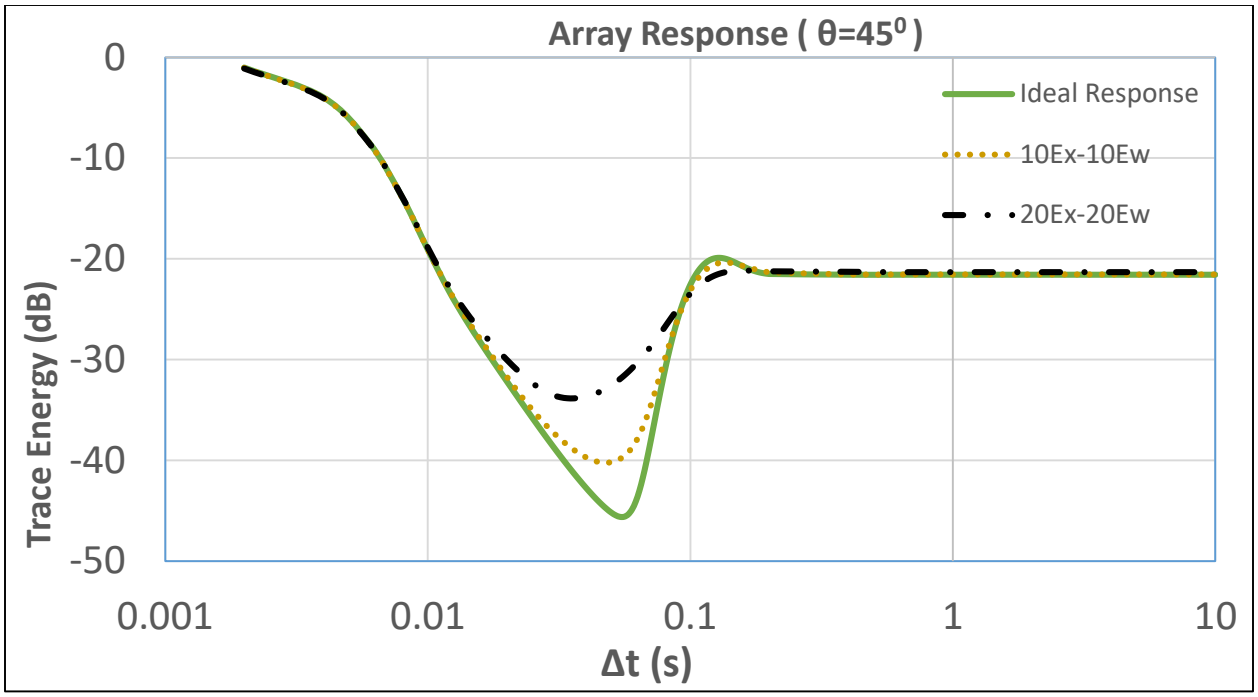

Figure *4*.**15.** Comparison between the ideal array and perturbed array responses with 10% and 20% standard deviation errors in elements' position and weight.

4.6. Trace energy of the array response with combined errors in the elements' elevation and weights.

Figures 4.16, 4.17, and 4.18 show the trace energy of the array response affected by combined errors of elements' elevation and weight. Figures 4.16 and 4.17 show three-dimensional surfaces, which represent trace energy of perturbed array response affected by 10% and 20% standard deviation errors in the elements' elevation and weight, respectively. As mentioned earlier, if the responses were related to elevation error, the degradation of the perturbed array response appeared in small incidence angle.

Through the observation of trace energy in the two-dimensional curves (Figure 4.18), the perturbed array response caused by 10% of the combined errors degraded 15% of ideal array response. Meanwhile, 20% of the combined errors degraded 26% of trace

energy. This implies that the weight errors had a small effect on combined errors as compared to the elevation errors.

This case has similar degradation as compared to the case of combined effect of element's position and weight error. The degradation of trace energy tolerates 7% error for each type to achieve acceptable trace energy.

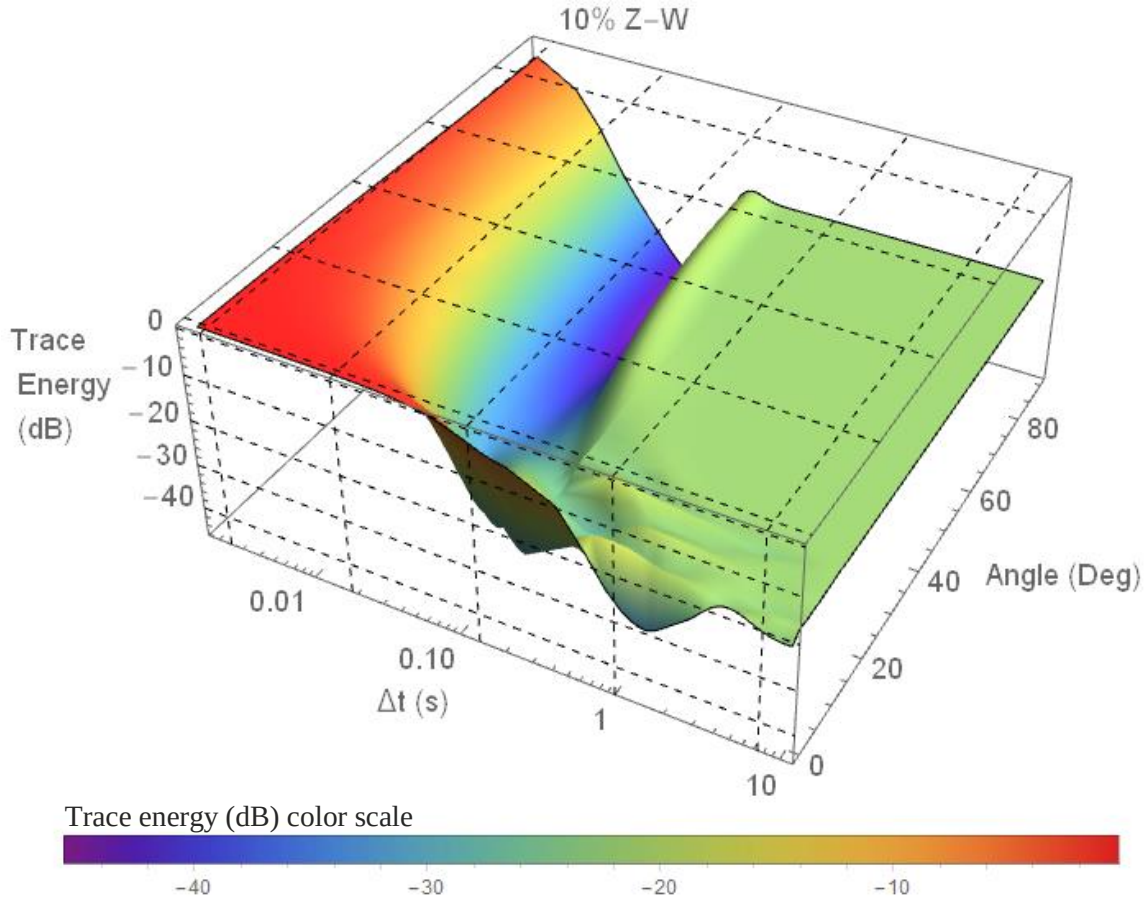

Figure *4.16.* A three-dimensional surface representing the trace energy of perturbed array response affected by 10% standard deviation errors in elements' elevation and weight with various incidence angles (θ=0º - 90º).

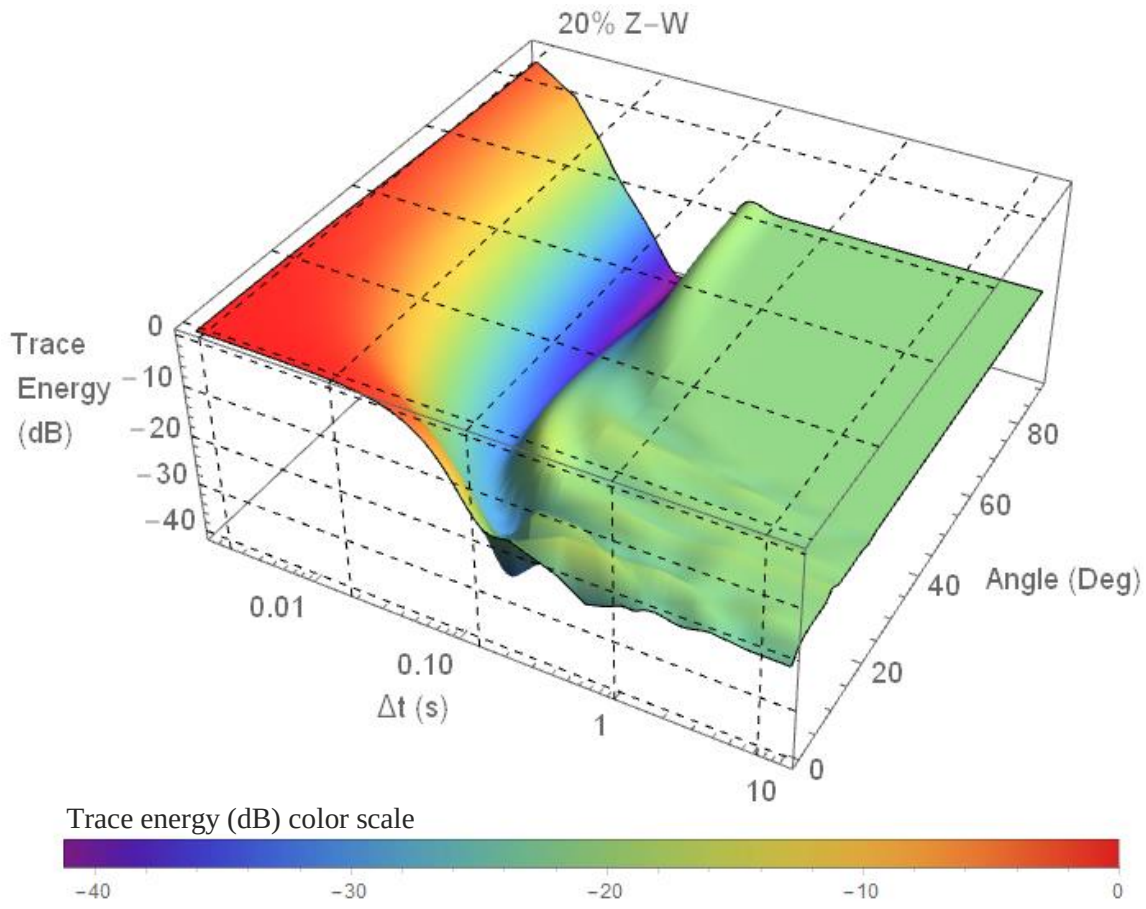

Figure 4.17. A three-dimensional surface representing the trace energy of perturbed array response affected by 20% standard deviation errors in elements' elevation and weight with various incidence angles (θ=0º - 90º).

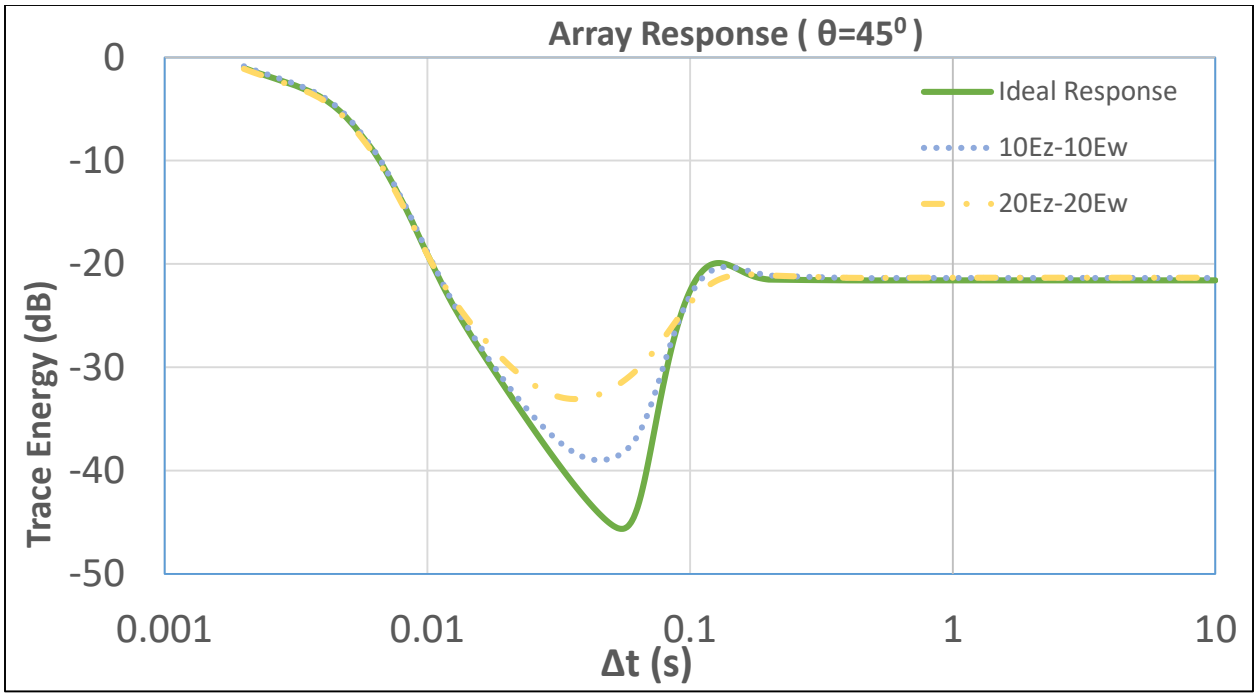

Figure 4.18. Comparison between the ideal array and perturbed array responses with 10% and 20% standard deviation errors in elements' elevation and weight.

4.7. Trace energy of the array response with combined errors in the elements' position, elevation, and weights.

Figures 4.19, 4.20, and 4.21 show the trace energy of the array response affected by combined errors of elements' position, elevation, and weight. Figures 4.19 and 4.20 show three-dimensional surfaces, which represent trace energy of perturbed array response affected by 10% and 20% standard deviation errors in the elements' position, elevation, and weight respectively. The perturbed array response was expected to be the most affected wavelet responses by these combinations of errors.

Moreover, the two-dimensional curve (Figure 4.21) at 45° incidence angle present significant degradation, especially in 20% added errors. These combined errors degraded

up to 30% of trace energy of the ideal array. In the other case, the addition of 10% combined errors to the ideal case caused 17% degradation of the minimum trace energy.

The degradation of trace energy will be more acceptable, which is less than 10% degradation if the error in each type of error is less than 5% from the ideal condition.

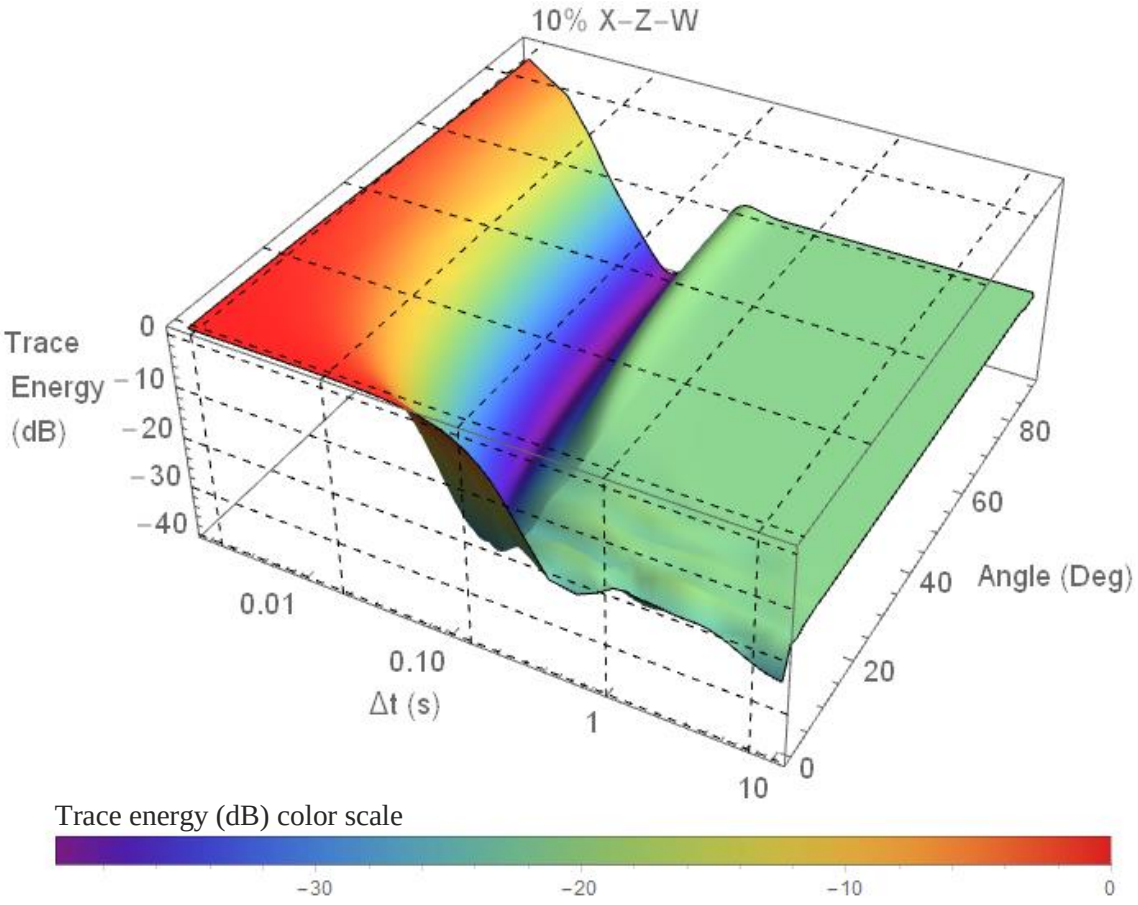

Figure *4*.19. A three-dimensional surface representing the trace energy of perturbed array response affected by 10% standard deviation errors in elements' position, elevation, and weight with various incidence angles (θ=0º - 90º).

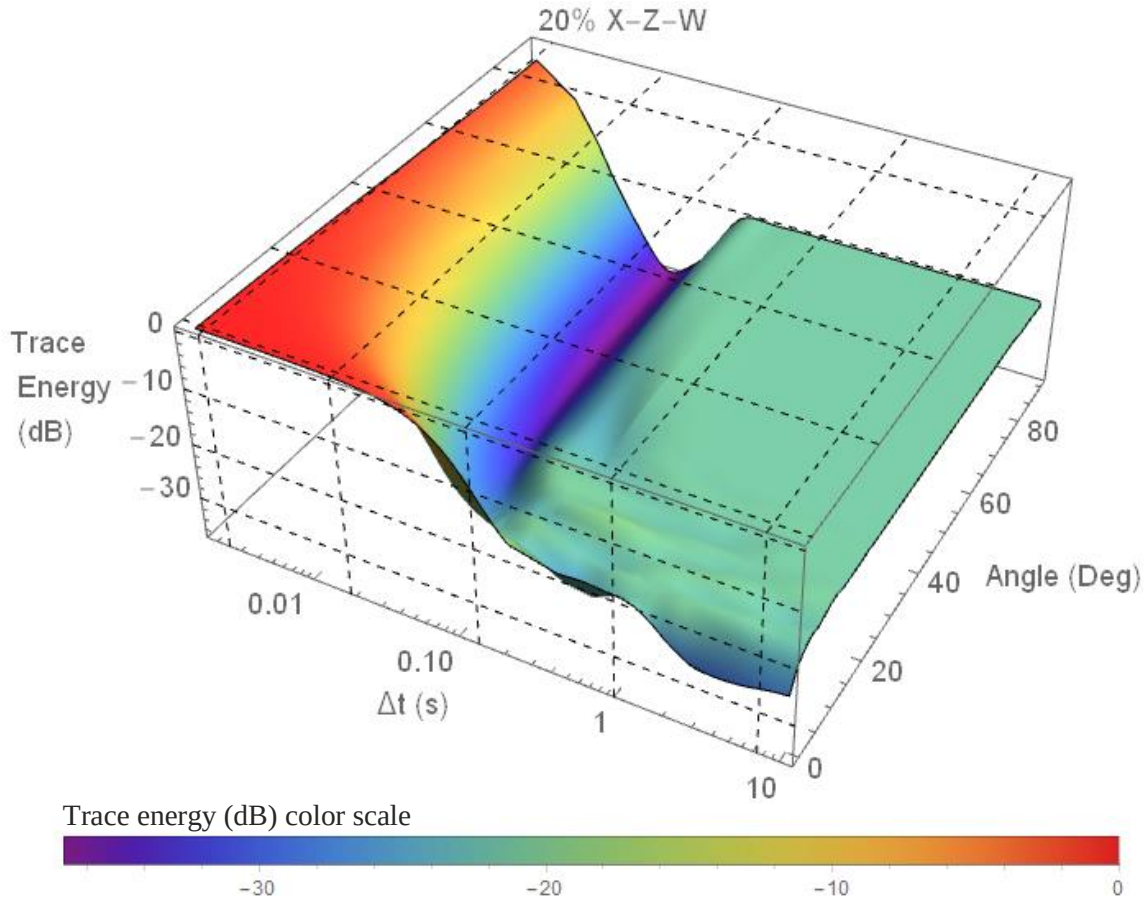

Figure *4*.**20.** A three-dimensional surface representing the trace energy of perturbed array response affected by 20% standard deviation errors in elements' position, elevation, and weight with various incidence angles (θ=0º - 90º).

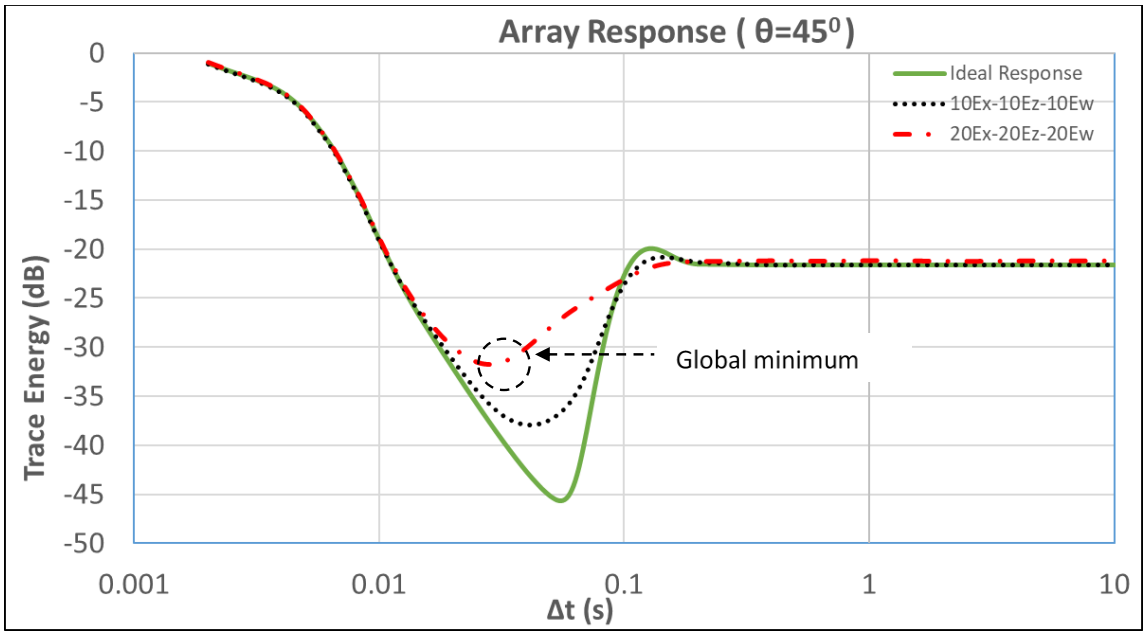

Figure *4.*21. Comparison between the ideal array and perturbed array responses with 10% and 20% standard deviation errors in elements' position, elevation, and weight.

Figure 4.22 summarizes the percentages of trace energy degradation for each model. The observation was a focus on the global minimum point.

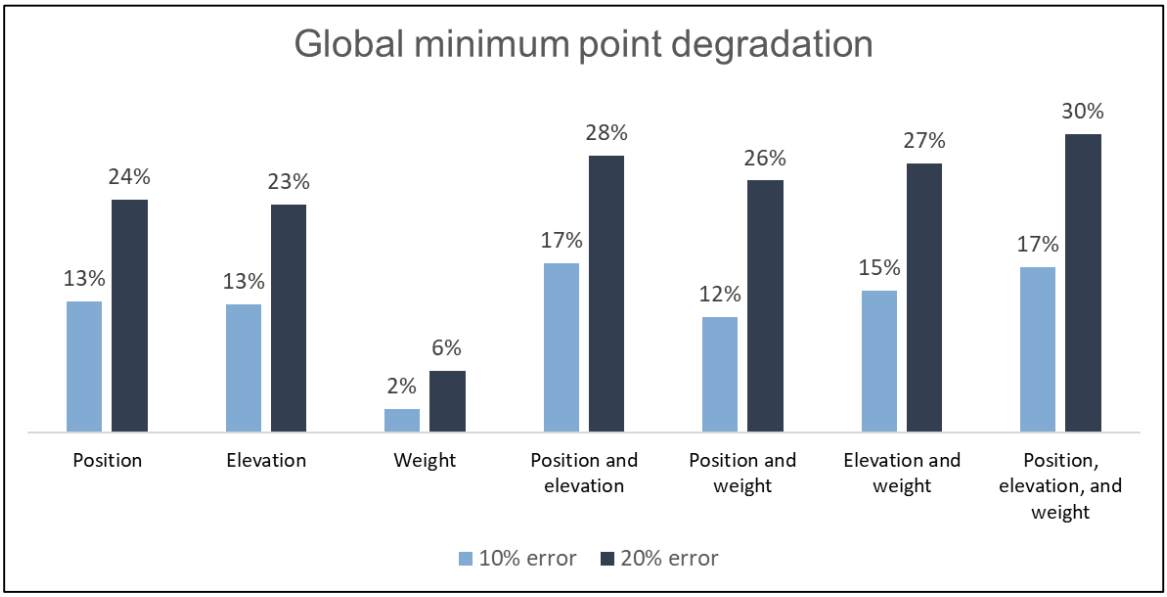

Figure *4.*22. The percentages of trace energy degradation of all the cases throughout the study.

CHAPTER 5

APPLICATION ON REAL DATA

In this chapter, I investigated the error in elements' positions, elevations, and weights on real data. The purpose of this investigation is to explain how to apply the methodology on real data.

5.1. Data acquisition

The 2D seismic data was acquired at KFUPM beach located in eastern Saudi Arabia in the Fall of 2011. The first receiver was located 10 meters away from the shoreline. The geological setting was a sand dune over Sabkha. Figure 5.1 shows the 2D seismic line from South West to North East. Originally, there was not any building around the seismic line when the seismic data was acquired in 2011.

Figure 5.2 illustrates the location of receivers and source along the 2D seismic line. The seismic line consists of 1 source point and 22 receiver points. The positions and elevations for each point were measured using *Differential Global Positioning System* (DGPS) with errors of 0.5 to 1 centimeters. The ideal spacing between the receivers was 5 meters and the source point was located 15 meters ahead of the first (SW) receiver along the line. The source of the seismic data was a hammer plugged in to the *Geometric Geode.* The seismic data were recorded for 0.5 seconds with 0.5 milliseconds sampling interval.

Noise level during data acquisition was very low because the area was far from the main road and wind speed was relatively low.

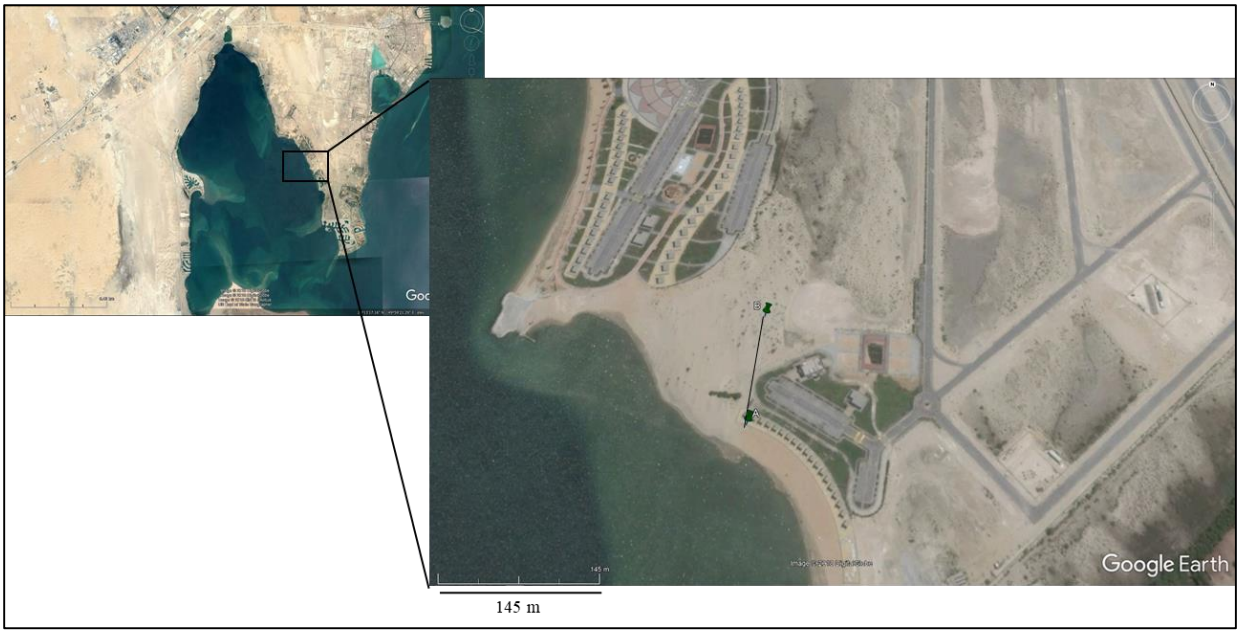

Figure 5.1. Seismic data was taken on KFUPM beach, Al-Khobar. The seismic line was located 10 meters from the sea with SW-NE direction.

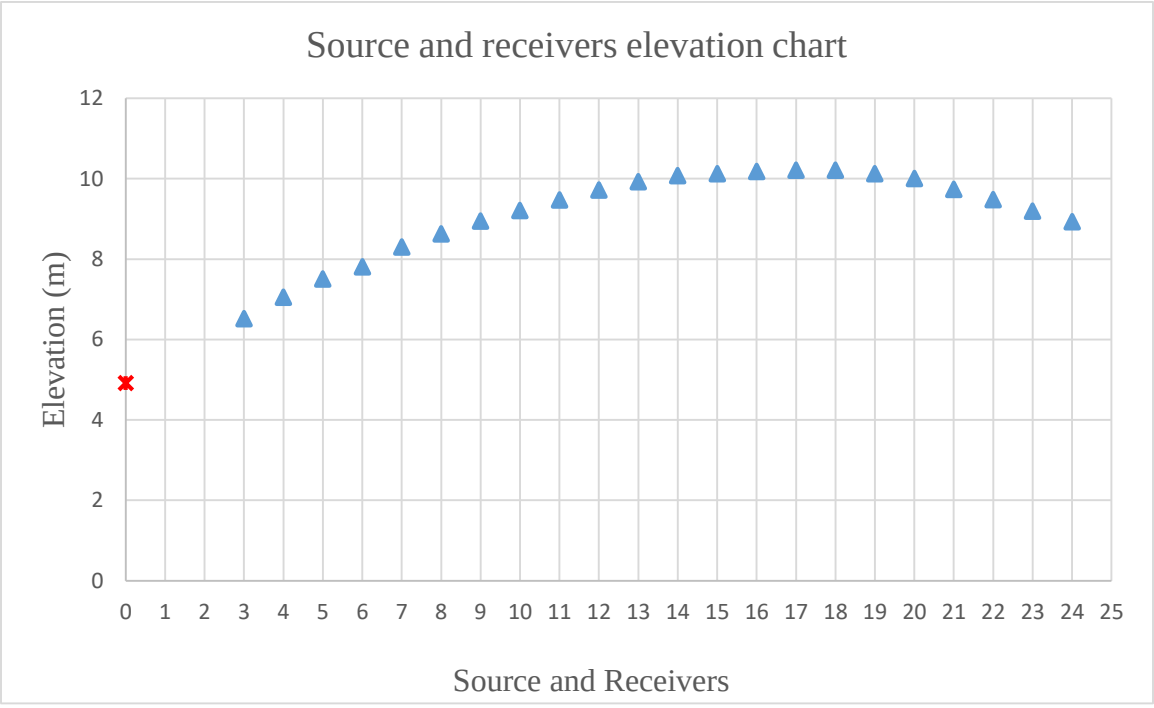

Figure 5.2. An elevation chart of the source (red) and receivers (blue) on 2D seismic line.

5.2. Methodology

In the application of synthetic data, trace energy was used to quantify the percentage of error affected by variations of positions, elevations, and weight of the elements. To calculate the normalized trace energy, as written in Equation 2.8, it needs the ideal trace energy, the perturbed trace energy, and the trace energy at Δt=0.

There were variations in elements' elevation on acquired seismic data as seen in Figure 5.2. The ideal distance between the elements was 5 meters, however, the elements were not planted at exactly 5 meters between each of them. The location of elements were measured using measuring tape, then after the elements had been planted, the exact coordinates were measured using DGPS. Hence, there were small errors in the elements' positions. The other variation was the ground coupling. Each element might have been planted with different ground coupling, thus, it made variations of elements' weights. Therefore, the acquired seismic data was considered as the perturbed wavelet response due to the presence of errors in elements' elevations, positions, and weights.

Since the seismic data had 0.5 seconds length, I limited the observation within a certain window for each trace to simplify the calculation. I followed the following steps to analyze the data:

1) Picking the arrival time of head wave for each trace as the arrival time of the perturbed wavelet ($\boldsymbol{t_{obs}}$)
2) Taking a time window ±0.005 seconds (10 samples) from the arrival time
3) Calculating the trace energy of the perturbed wavelet response
4) Generating the ideal wavelet response by shifting the $\boldsymbol{t_{obs}}$ and producing $\boldsymbol{t_{shift}}$.
5) Calculating the trace energy of the ideal wavelet response

6) Generating the ideal wavelet response at $\Delta t = 0$ by shifting t_{shift} as if they arrived at the same time

7) Calculating the trace energy of the ideal wavelet response at $\Delta t = 0$

8) Analyzing the percentage of error in the perturbed-array wavelet response

5.2.1. The trace energy of the perturbed wavelet response

The perturbed wavelet response was represented by the acquired seismic data. The first step to calculate the trace energy was picking the arrival time (t_{obs}) of 22 traces from the seismic data (Figure 5.3). The observation was focused on the arrival time of the head wave because it suffers more from variations in the near-surface.

The trace energy was represented on Equation 2.7 as the sum of the squared amplitudes from each trace. Hence, the seismic data was extracted to get the amplitudes of every traces. To simplify the calculation of trace energy, each trace was windowed ±0.005 seconds (10 samples), therefore the number of samples was reduced from 1,000 samples to 21 samples around the arrival time.

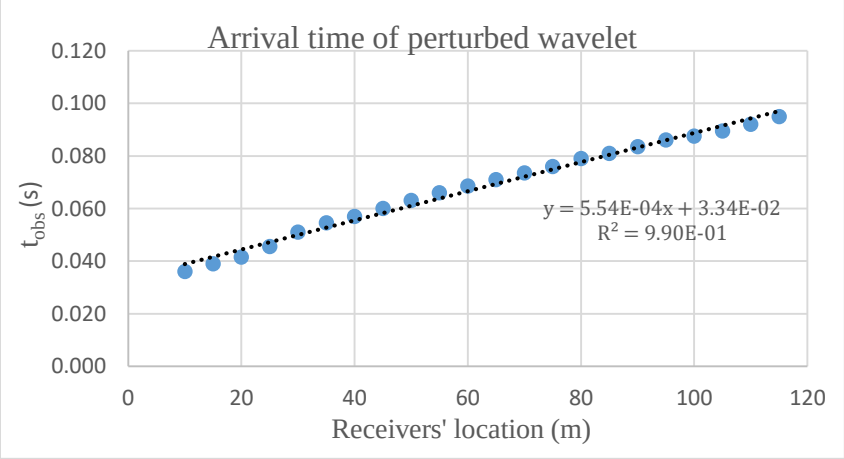

Figure 5.3. The observed arrival time picked from the seismic data (perturbed wavelet). The dotted line is the best-fit line with its equation and correlation coefficient shown as well.

Figure 5.4 shows the amplitude of the seismic data limited around the arrival time. The next step was summing the amplitude within each time sample then squaring each of them. The trace energy was the total of the squared amplitudes and the result was $\mathbf{3.10 \times 10^{11}}$.

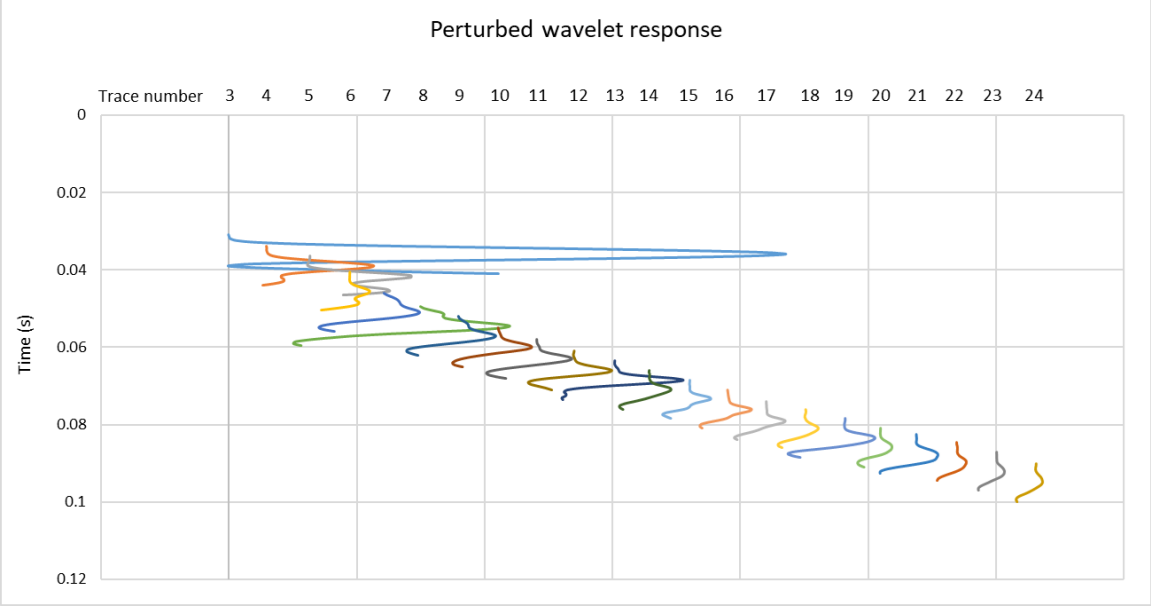

Figure 5.4. The amplitude of perturbed wavelet response in ±0.005 seconds time window for every trace.

5.2.2. The trace energy of the ideal wavelet response

The ideal wavelet response means the wavelet response without any errors in elements' positions, elevations, and weights. I generate the ideal wavelet response by adjusting the current seismic data (perturbed wavelet) as if it is acquired with ideal parameters. The method was to fit the arrival time of perturbed wavelet response using linear regression approach (Figure 5.5). Then, the seismic traces were shifted from t_{obs} to t_{shift} (Figure 5.6). In the end, the trace energy of ideal wavelet response was calculated using the same method as used previously on the perturbed wavelet response by summing the

squared amplitudes of the traces for each time sample. The trace energy of the ideal wavelet response was $\mathbf{3.04 \times 10^{11}}$.

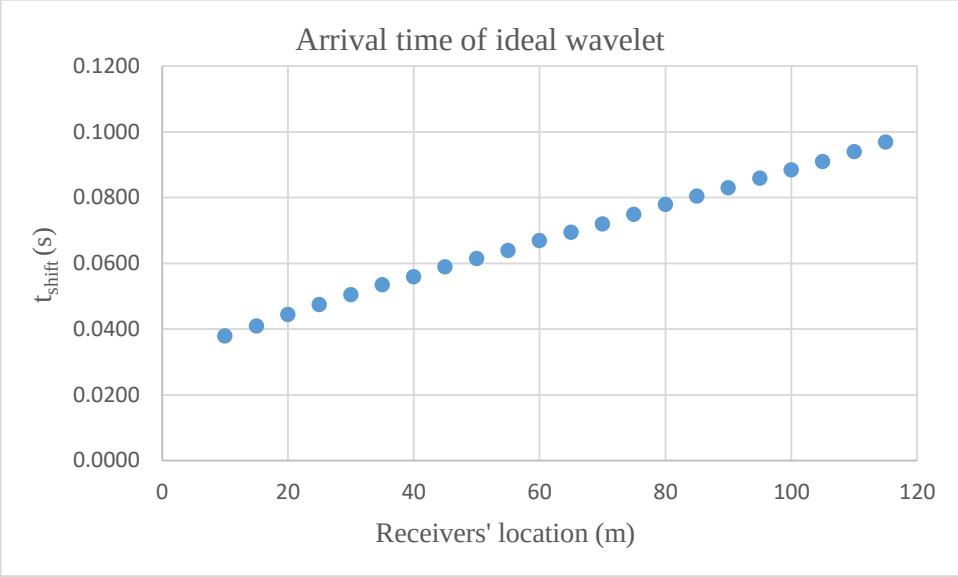

Figure 5.5. The shifted arrival times from the observed arrival times.

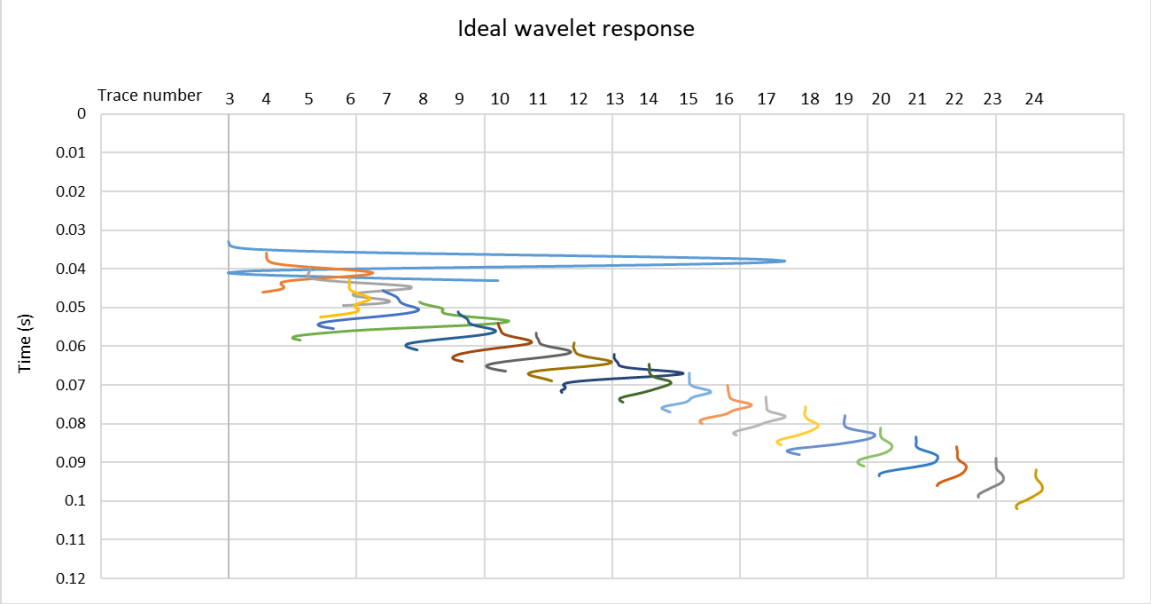

Figure 5.6. The amplitude of ideal wavelet response in ±0.005 seconds time window for every trace.

5.2.3. The trace energy of the ideal wavelet response at $\Delta t = 0$

The trace energy of the ideal wavelet response at $\Delta t = 0$ was calculated to find the normalized trace energy using Equation 2.8. $\Delta t = 0$ occurs when all the elements are planted in the same position, in which case the seismic wave will be received by the elements at the same time. To simulate this case, all the traces which already positioned at t_{shift} previously were shifted again, hence all the wavelets were located at same arrival time (Figure 5.7). Finally, similar to the previous method, the trace energy of the ideal wavelet response at $\Delta t = 0$ was calculated and the result was $\mathbf{1.23 \times 10^{12}}$.

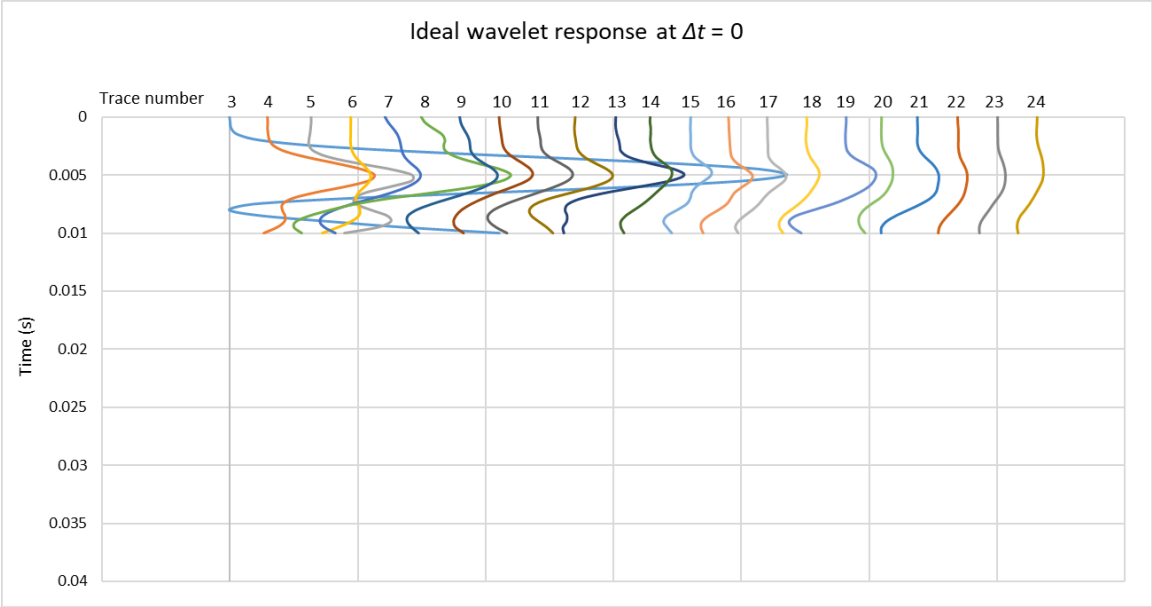

Figure 5.7. The amplitude of perturbed wavelet response at $\Delta t = 0$ in ±0.005 seconds time window for every trace.

5.3. The trace energy degradation

The comparison between the perturbed and ideal wavelet response was performed to quantify the degradation of the wavelet response on the real data. Firstly, the normalized

trace energies in dB scale for each case were calculated using Equation 2.9. Here is the result of the ideal wavelet response:

$$E_n = \frac{E(t)}{E(t=0)} = \frac{3.04 \times 10^{11}}{1.23 \times 10^{12}} = 0.248$$

$$E_n' = 20 \log_{10} E_n \ = 20 \log_{10}(0.248) = \mathbf{-12.094\ dB}$$

Moreover, here is the result of the perturbed wavelet response:

$$E_n = \frac{E(t)}{E(t=0)} = \frac{3.10 \times 10^{11}}{1.23 \times 10^{12}} = 0.253$$

$$E_n' = 20 \log_{10} E_n \ = 20 \log_{10}(0.253) = \mathbf{-11.938\ dB}$$

Therefore, the percentage of degradation of the wavelet response in the addition of errors in elements' positions, elevations, and weights is:

$$\%Error = \frac{E_n'\ ideal - E_n'\ perturbed}{E_n'\ ideal} \times 100\%$$

$$\%Error = \frac{(-12.094) - (-11.938)}{-12.094} \times 100\% = 1.29\%$$

This means that the combined errors of elements' positions, elevations, and weights on the real data degraded the trace energy of the wavelet response by **1.29%**.

5.4. Prediction based on current study

In the previous sections, I presented the degradation of the wavelet response caused by errors in elements' positions, elevations, and weights using the real data. In this section, the degradation of trace energy is predicted using to the method described in the previous chapters. To produce a fair prediction, the investigation uses the parameters of the real data.

There are several parameters which affected the calculation of the wavelet response as written in Equation 3.6, such as incidence angle (θ), number of elements (N), nominal spacing between elements (Δx), near-surface velocity (V), and the amount of errors in positions (Ex), elevations (Ez), and weights (Ew). The real seismic data was acquired using N=22 elements and a nominal distance between elements Δx=5 meters.

5.4.1. Near-surface velocity (V)

Near-surface velocity was used to calculate the trace energy of the wavelet response. The velocities below each element were calculated and the median was used as the near-surface velocity for further process. The first step to estimate the reference plane (datum) from known elements' elevations. In this study, the datum was found out to be dipping illustrated in Figure 5.8.

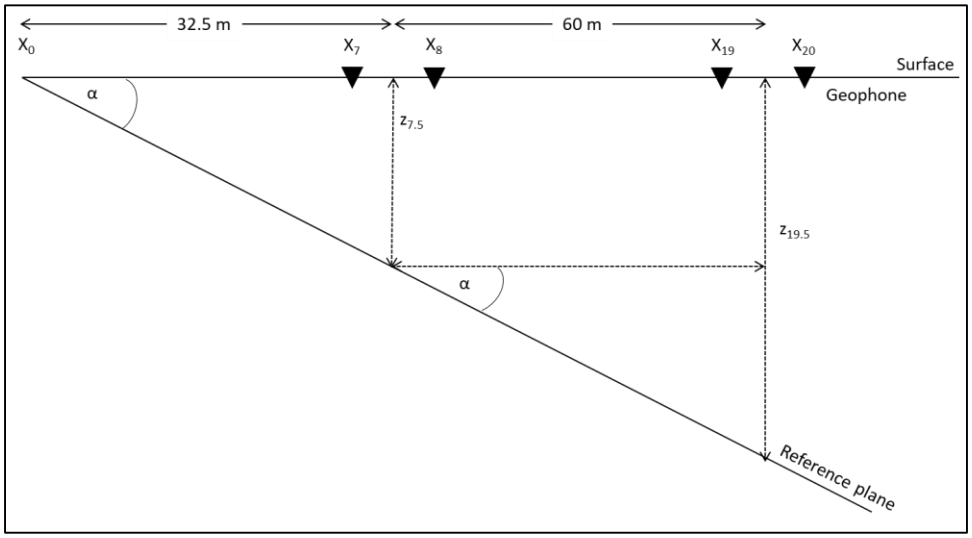

Figure 5.8. Illustration of the dipping reference plane (datum). Subscripts of x and z indicate receiver number (e.g., 7.5 means position between receivers 7 and 8).

The elements were not always located above datum, some of them were located below datum. In the beginning, the elements were located below datum, then after the 5th

element, the elements were located above datum until they reached the 17th element. After that, the elements were located below datum again until the last element (Figure 5.9). This analysis was deduced from the straight-line fit in Figure 5.3.

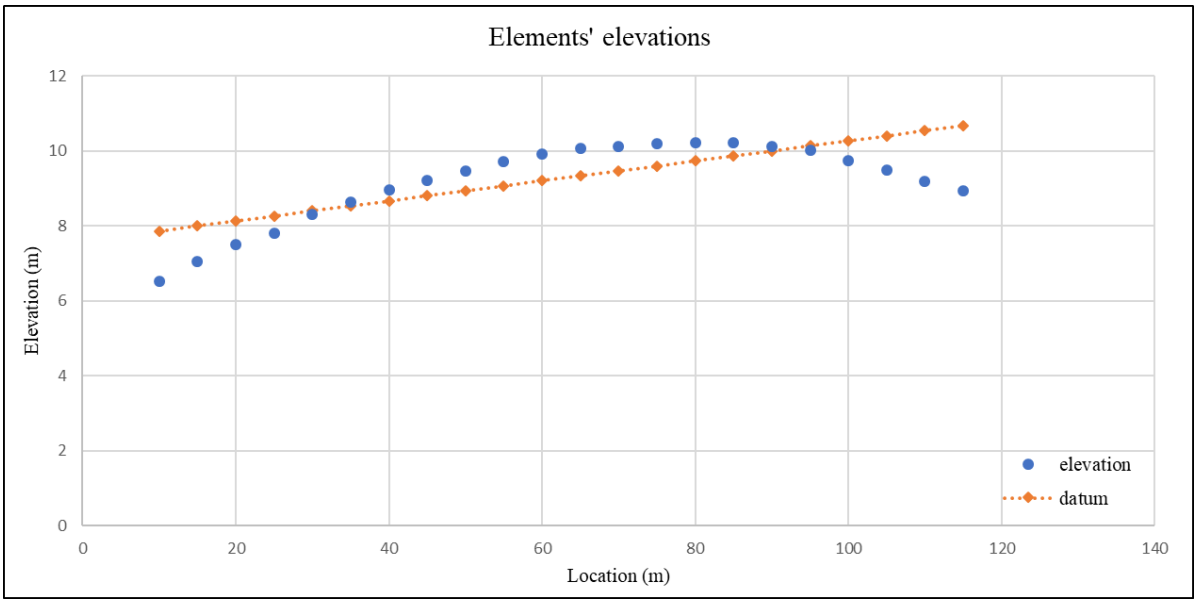

Figure 5.9. The elements' elevations along the seismic line (blue circle) and the reference plane (orange diamond).

The datum elevation for each element was calculated by the equation:

$$\boldsymbol{Datum = z_n + (x_n - 32.5)\tan(\alpha)} \tag{5.1}$$

where z_n and x_n are the elevation and position of the elements, respectively; and α=1.53° is the dipping angle of the reference plane.

Furthermore, to obtain the velocity of the near-surface layer (sand dune), the difference between datum and element elevations (*dz*) was divided by the difference between observed and calculated arrival times (*dt*):

$$V_1 = dz/dt.$$

(5.2)

The calculated arrival time was estimated from the head-wave arrival at the nth element using the equation:

$$t_{calc\_n} = t_i + \frac{x_n}{V_2}.$$

(5.3)

where t_i = 0.0334 seconds is the head-wave intercept obtained from fitting the best-fit line to t_{obs} and V_2 = 1805 m/s was calculated from the slope of the best-fit line to t_{obs}.

The results for V_1 are shown in Table 1 and the median velocity was **403 m/s**, which was considered as V_1 and used for the further analysis. It can be seen from Table 1 that some velocities are erroneous probably due to picking errors caused by noise and wavelet non-stationarity. The median velocity was used instead of the mean because it is more representative of the data (i.e., 50% of the data are below and 50% are above it) and is not affected by outliers as we have in this case.

Table 5.1. Near-surface velocity obtained for every trace and the median of the data considered as V_1.

Trace #	x (m)	z (m)	t_{obs} (s)	t_{calc} (s)	dt (m)	datum (m)	dz (m)	V_1 (m/s)
3	10	6.518	0.036	0.0389	-0.0029	7.867	-1.349	462
4	15	7.052	0.039	0.0417	-0.0027	8.001	-0.949	353
5	20	7.511	0.042	0.0445	-0.0030	8.134	-0.623	211
6	25	7.812	0.046	0.0472	-0.0017	8.268	-0.456	264
7	30	8.303	0.051	0.0500	0.0010	8.401	-0.098	-98
8	35	8.633	0.055	0.0528	0.0017	8.535	0.098	57
9	40	8.951	0.057	0.0555	0.0015	8.668	0.283	193
10	45	9.211	0.060	0.0583	0.0017	8.802	0.409	242
11	50	9.475	0.063	0.0611	0.0019	8.935	0.540	281
12	55	9.722	0.066	0.0638	0.0022	9.069	0.653	303
13	60	9.931	0.069	0.0666	0.0019	9.202	0.729	387
14	65	10.075	0.071	0.0694	0.0016	9.335	0.740	458
15	70	10.129	0.074	0.0722	0.0013	9.469	0.660	491
16	75	10.183	0.076	0.0749	0.0011	9.602	0.581	540
17	80	10.211	0.079	0.0777	0.0013	9.736	0.475	364
18	85	10.212	0.081	0.0805	0.0005	9.869	0.343	639
19	90	10.129	0.084	0.0832	0.0003	10.003	0.126	473
20	95	10.010	0.086	0.0860	0.0000	10.136	-0.126	49678
21	100	9.737	0.088	0.0888	-0.0013	10.270	-0.533	419
22	105	9.479	0.090	0.0915	-0.0020	10.403	-0.924	453
23	110	9.194	0.092	0.0943	-0.0023	10.537	-1.343	581
24	115	8.930	0.095	0.0971	-0.0021	10.670	-1.740	836

5.4.2. Incidence angle (θ)

In the previous section, V_1 and V_2 were already obtained. The incidence angle was the critical angle calculated as:

$$\boldsymbol{\theta = \sin^{-1}\left(\frac{V_1}{V_2}\right)} \tag{5.4}$$

The result of above calculation was $\boldsymbol{\theta = 12.6^{o}}$.

5.4.3. Errors in elements' positions (*Ex*)

The distance between the elements was nominally 5 meters and it was measured using measuring tape. Therefore, after the actual coordinates were measured using DGPS, there was a small margin of errors between the actual distances and the nominal distance between the elements. Figure 5.10 shows the deviations of the actual elements' positions from the ideal positions during the seismic acquisition. To calculate the actual distance between adjacent elements from measured coordinates, the equation below was used:

$$\boldsymbol{D = \sqrt{(x_2 - x_1) + (y_2 - y_1)},} \tag{5.5}$$

where (x_1,y_1) and (x_2,y_2) are the DGPS coordinates of the two adjacent elements.

The errors in elements' positions were calculated using Equation 3.3 where Δx_n is the difference between the observed and ideal distances. The results of Ex_n from every trace are shown in Table 2, which were used in further steps to calculate the perturbed wavelet response.

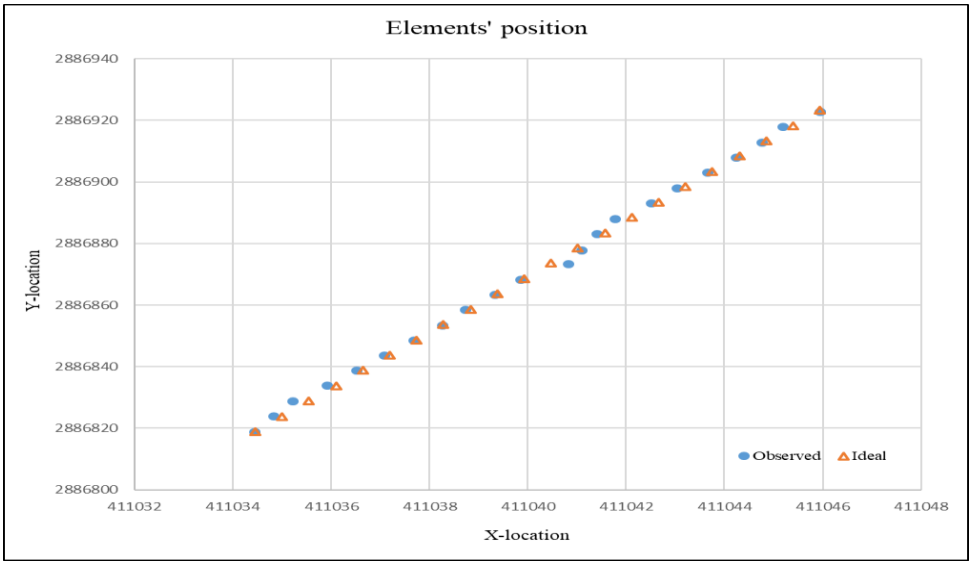

Figure 5.10. The position of the elements during seismic acquisition measured by DGPS equipment (blue circle) and the ideal location with equal distance between the elements (orange triangle).

Table 5.2. Coordinates of the elements' positions, the actual distances, and the errors in elements' positions (Ex_n)

Trace	X	Y	Distance (m)	ΔX_n	Ex_n
Reference	411034	2886814			
3	411034	2886819	4.955	0.045	0.90%
4	411035	2886824	4.951	0.049	0.97%
5	411035	2886829	5.010	-0.010	-0.20%
6	411036	2886834	5.058	-0.058	-1.17%
7	411037	2886839	4.919	0.081	1.62%
8	411037	2886843	4.831	0.169	3.37%
9	411038	2886849	5.047	-0.047	-0.93%
10	411038	2886853	4.866	0.134	2.69%
11	411039	2886858	5.088	-0.088	-1.76%
12	411039	2886863	4.875	0.125	2.51%
13	411040	2886868	5.022	-0.022	-0.45%
14	411041	2886873	5.079	-0.079	-1.57%
15	411041	2886878	4.631	0.369	7.37%
16	411041	2886883	5.285	-0.285	-5.70%
17	411042	2886888	4.873	0.127	2.54%
18	411043	2886893	5.078	-0.078	-1.55%
19	411043	2886898	4.969	0.031	0.62%
20	411044	2886903	5.103	-0.103	-2.07%
21	411044	2886908	4.921	0.079	1.58%
22	411045	2886913	4.872	0.128	2.56%
23	411045	2886918	5.200	-0.200	-4.01%
24	411046	2886923	4.916	0.084	1.68%

5.4.4. Errors in elements' elevations (*Ez*)

The elevations along the seismic line were different for each element's point as shown in Figure 5.2. The elevation increased until it reached the maximum elevation at the 18^{th} element then it decreased until the last trace. This condition affected the arrival times

of the wavelet from the subsurface. To figure out the amount of errors in each element's elevation, similar procedures to the elements' position was used. The assumption was made for the reference of ideal elevation to use the datum described in Section 5.4.1 (Figure 5.9).

The errors in elements' elevations (Ez_n) were calculated using Equation 3.4 where z_n is the difference between the observed and reference elevations (Figure 5.11)

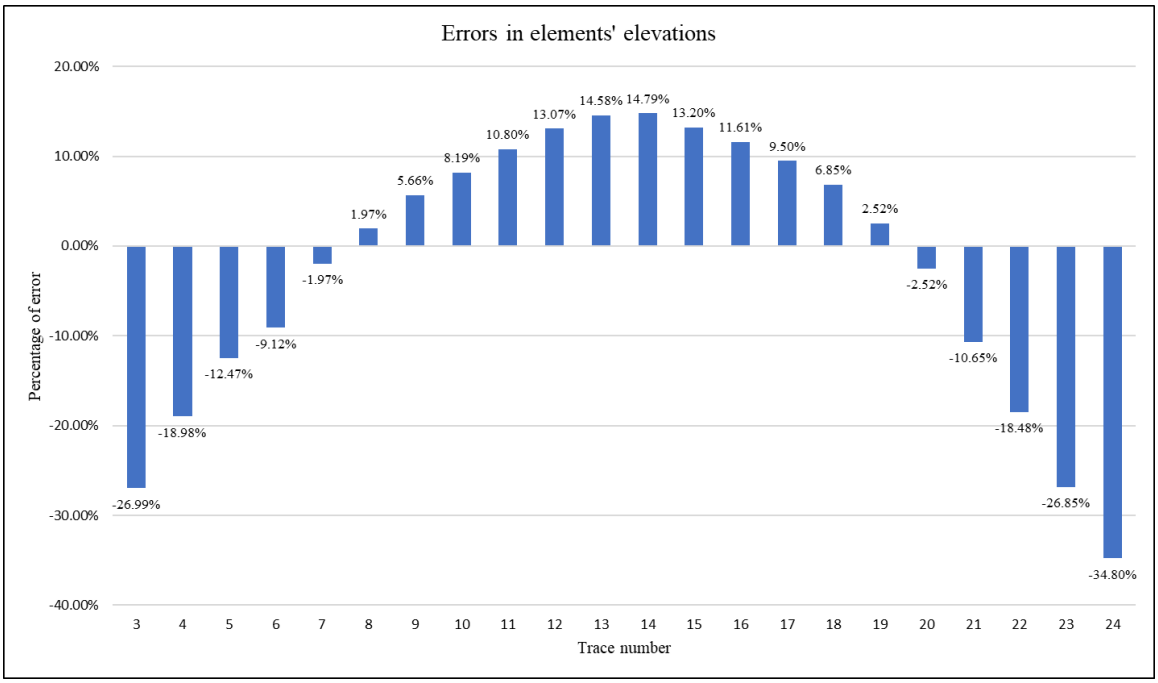

Figure 5.11. Percentage of error in elements' elevation obtained by dividing the difference between the observed and reference elevations (z_n) by the ideal distance between the elements (Δx).

5.4.5. Errors in elements' weights (*Ew*)

The errors in elements' weights were more complicated to determine compared to the errors in elements' positions and elevations. The problem occurred mainly when making the assumption of the ideal weights within the seismic data. In this study, I decided to use the absolute mean trace as the reference or the ideal weight to be compared to all the amplitudes in each trace.

Since the amplitudes of the traces were very diverse, physical gain method to the seismic data was applied. The time-power gain method was selected to be applied to the data.

$$\boldsymbol{A_0 = A(t) \times t^{\alpha}} \tag{5.6}$$

where $\alpha = 2$ to account for both geometrical spreading and from attenuation [23]. Figure 5.12a shows the traces after time-power gain application.

The next step was taking the absolute values for each trace to generate the absolute mean trace by calculating the mean of each time sample (Figure 5.12b). Then, the median amplitude of the absolute mean trace and the median amplitude of each absolute trace were calculated. Ew_n were considered as the percentage of error between the median of each absolute trace with respect to the median of the absolute mean trace (Figure 5.13).

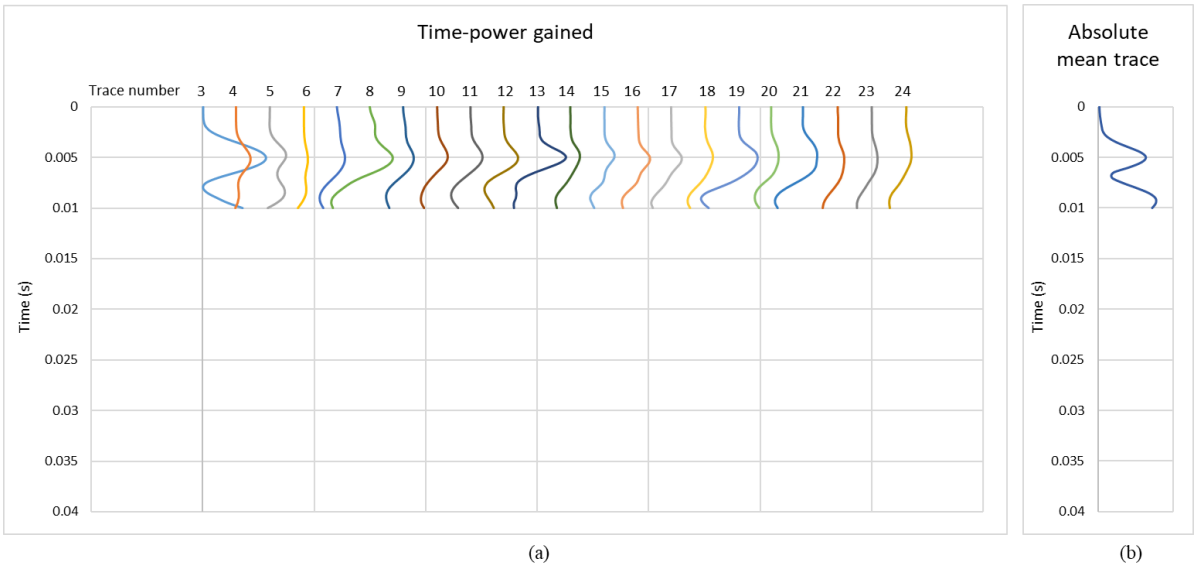

Figure 5.12. (a) Time-power gained amplitude for each trace along the seismic line and (b) the absolute mean trace obtained by taking the absolute mean value for every time sample.

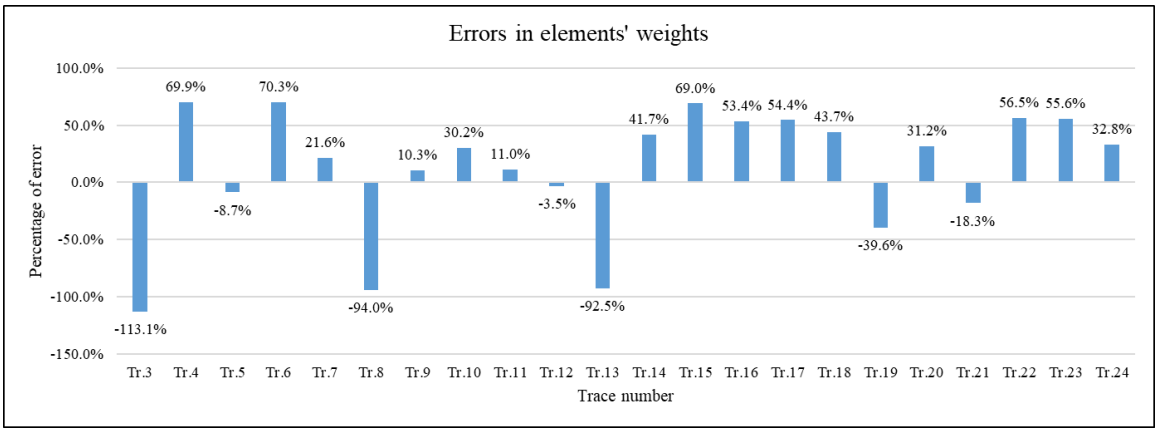

Figure 5.13. The amount of errors in elements' weights (Ew_n) calculated by comparing the median of time-power gained amplitude for each absolute trace and the median of the absolute mean trace.

5.4.6. Prediction of the trace energy of the real data

After the parameters needed to calculate the wavelet response had been obtained as explained in the previous sections, the wavelet responses were calculated using Equation 3.6. The methodology used here were similar compared to the previous chapters. However, since the amount of errors for individual element were actually calculated, the Gaussian distribution was not utilized to generate them.

Moreover, the normalized trace energies were calculated using Equation 2.8 and 2.9. The result showed that the normalized trace energy for the perturbed wavelet response was **-31.99 dB**. Meanwhile, the normalized trace energy of the ideal wavelet response was **-51.80 dB**. The degradation of the wavelet response due to errors in elements' positions, elevations, and weights was **38.24%.**

The degradation of trace energy predicted by the method was significantly different from that calculated directly from the real data, which was 1.29%. There are several reasons that may cause the significant difference. The application of method used the assumption that the incident wavelet was zero-phase Ricker wavelet. On the other hand,

the real data was acquired using hammer which may have a minimum-phase or mixed-phase wavelets. The amount of errors in elements' position assumed that the actual elements were planted along the line, however, Figure 5.10 showed that there were some offsets perpendicular to the seismic line. The presence of noise in the real data (which was not present in the prediction calculation) might have contributed to this discrepancy. In addition, the 2-squared method used to gain the data might not be sufficient to account for attenuation in the loose sand dune. These assumptions could have affected the calculation of the predicted value of the trace energy degradation, hence the results were different compared to the trace energy degradation on real data.

CHAPTER 6

CONCLUSIONS AND RECOMMENDATIONS

6.1. Conclusions

The objective of this study was to investigate the changes in the wavelet response of seismic arrays in the presence of combined errors in elements' elevations, positions, and weights within the array. As a result, at 45º incidence angle, the minimum array response in the ideal case has a trace energy of -43 dB which occurs at a temporal element spacing of 0.054 s. The addition of 10% single error in each position, elevation, and weight caused the global minima of array responses to degrade by 13%, 13%, and 2% respectively. Combining the three of them will degrade array responses by 17% from the ideal response. Meanwhile, adding 20% standard deviation error for position, elevation, and weight separately degrades the global minima of array responses by 24%, 23%, and 6%, respectively. If three of them are combined, the array responses will degrade by 30% from the ideal response.

In summary, the conclusions of this study are:

1. Studying seismic array responses is very useful in understanding the effects of different variations.
2. As expected, the combination of errors greatly degraded the array response as compared to individual error. However, it does not necessarily indicate that the degradation of combined errors is the total degradation of each individual error.
3. The effects of combined errors are substantial and care must be taken into account in planting arrays as close to the ideal case as possible.

4. Based on quantitative estimation, to reach optimum results in seismic data acquisition, errors in elements positions and elevations should not reach 7% from the ideal condition. This case will degrade only up to 10% of the trace energy.
5. The application of the methodology on the seismic real data is beneficial for this study. The benefit is to understand the procedure to extract the information from the seismic real data and the comparison between the results from the synthetic and real data.
6. The degradation of trace energies using real data (1.29%) were not exactly the same as predicted by the method (38.24%) with the same parameters. This might be due to several assumptions that were not satisfied by the real seismic data.

6.2. Recommendations

From the results of this study, the following are the recommendations for future research related to this study:

1. The real data application could be more practical if the seismic data are acquired on three configurations, which are the ideal condition, the applied-error configuration, and the configuration when the elements are located on the same position ($\Delta t = 0$). In this case, the result would be more suitable instead of modifying the acquired data.
2. The study will be closer to the real conditions if it includes intra-array heterogeneities in the near surface.

3. The study of array response using 2D arrays could be considered in future research. 2D array means that the elements are planted in 2D geometry instead of one line that used in this study.

REFERENCES

[1] D. F. Aldridge, "Statistically perturbed geophone array responses," *Geophysics,* vol. 54, pp. 1306-1318, 1989.

[2] S. Rost and C. Thomas, "Array seismology - methods and applications," *Review of Geophysics,* vol. 40, pp. 1-27, 2002.

[3] A. Douglas, D. Bowers, P. D. Marshall, J. B. Young, D. Porter and N. J. Wallis, "Putting nuclear-test monitoring to the test," *Nature,* vol. 398, pp. 474-475, 1999.

[4] A. Douglas, "Seismometer arrays—Their use in earthquake and test ban seismology," in *Handbook of Earthquake and Engineering Seismology,* H. K. a. W. L. P. Jennings, Ed., 2002, p. 357–367.

[5] H. Kárason and R. D. van der Hilst, "Tomographic imaging of the lowermost mantle with differential times of refracted and diffracted core phases (PKP, Pdiff)," *Journal of Geophysical Research,* vol. 106, p. 6569–6587, 2001.

[6] B. H. Hoffe, G. F. Margrave, R. R. Stewart, D. S. Foltinek, H. C. Bland and P. M. Manning, "Analyzing the effectiveness of receiver arrays for multicomponent seismic exploration," *Geophysics,* vol. 67, pp. 1853-1868, 2002.

[7] G. Li, H. Zheng, J. Wang and W. Huang, "Inversion-based directional deconvolution to remove the effect of a geophone array on seismic signal," *Journal of Applied Geophysics,* vol. 130, pp. 91-100, 2016.

[8] M. K. Smith, "Noise analysis and multiple seismometer theory," *Geophysics,* vol. 21, pp. 337-360, 1956.

[9] J. E. White, "Transient behavior of patterns," *Geophysics,* vol. 23, pp. 26-43, 1958.

[10] P. Newman and J. T. Mahoney, "Patterns-with a pinch of salt," *Geophysical Prospecting,* vol. 21, pp. 197-219, 1973.

[11] D. H. Johnson and D. E. Dudgeon, "Signal Processing - Concepts and Techniques," *Prentice-Hall Inc.,* 1993.

[12] A. F. Gangi and M. A. Benson, "The wavelet response of seismic arrays," *SEG Expanded Abstracts,* pp. 663-666, 1989.

[13] A. Al-Shuhail and A. F. Gangi, "The effect of topography on the wavelet response of the seismic arrays," *SEG Expanded Abstracts,* pp. 895-898, 1994.

[14] A. Al-Shuhail and A. Al-Ghanim, "Performance of seismic arrays in heterogeneous medium," *GeoFrontier,* vol. 1, pp. 27-30, 2003.

[15] A. Al-Shuhail, "Seismic array response in the presence of a dipping shallow layer," *SIViP,* vol. 7, pp. 263-274, 2011.

[16] J. Akram, "Seismic arrays response in the presence of laterally varying thickness of the weathering layer," *M.S. Thesis, KFUPM,* 2007.

[17] N. Ricker, "The form and laws of propagation of seismic wavelets," *Geophysics,* vol. 18, pp. 10-36, 1953.

[18] J. K. Costain and C. Coruh, Basic theory of exploration seismology, Elsevier, 2004.

[19] R. E. Sheriff and L. P. Geldart, Exploration Seismology. Vol. 1: History, Theory, and Data Acquisition, 1982.

[20] R. L. Sax, "Stationarity of seismic noise," *Geophysics,* vol. 33, pp. 668-674, 1968.

[21] M. A. Benson, "The impulse and wavelet responses of seismic arrays," *M.S. Thesis, Texas A&M University,* 1989.

[22] A. Al-Shuhail, "The Effect of topography on the wavelet response of seismic arrays," *M.S. Thesis, Texas A&M University*, 1993.

[23] J. F. Claerbout, Imaging the Earth's Interior, Blackwell Scientific Publications, 1985.

VITAE

First name : Ryan Adhi

Last name : Putra

Date of birth : October 2nd, 1989

Nationality : Indonesian

Email : ryanadhi.p@gmail.com

Address : Jln. Penganten Ali 3 No.44 Ciracas, Jakarta Timur, Indonesia 13740

Education :

King Fahd University of Petroleum and Minerals (KFUPM)

Master of Science in Geophysics, College of Petroleum Engineering and Geosciences

Graduated in 2017 (GPA 3.53/4)

Institut Teknologi Bandung (ITB)

Bachelor of Science in Geophysical Engineering, College of Petroleum and Mining Engineering

Graduated in 2012 (GPA 3.02/4)

Research	:	Microseismic data processing at The Center for Energy and Geo Processing (CeGP)
Publication	:	"*Seismic array response in the presence of intra-array variations in element weights, elevations, and positions*" by Putra, R.A. and Al-Shuhail, A.A. presented in GEO 2018 Conference, Bahrain.
Work experience	:	Geophysicist at PT. Quest Geophysical Asia (2013 – 2014)